THE JOURNAL OF PHYSICAL CHEMISTRY B

ARTICLE

pubs.acs.org/JPCB

Strong Electronic Correlation Effects in Coherent Multidimensional Nonlinear Optical Spectroscopy

M. E. Karadimitriou,[†] E. G. Kavousanaki,[‡] K. M. Dani,[§] N. A. Fromer,[∥] and I. E. Perakis*[,†]

[†]Department of Physics, University of Crete, Heraklion, Crete, 71003, Greece, and Institute of Electronic Structure & Laser, Foundation for Research and Technology-Hellas, Heraklion, Crete, 71110 Greece

[‡]Department of Physics, University of Konstanz, D-78464 Konstanz, Germany

[§]Center for Integrated Nanotechnologies, Los Alamos National Laboratory, New Mexico, 87545 United States

[∥]California Institute of Technology, 1200 E California Blvd, MC 107-81, Pasadena, California 91125, United States

ABSTRACT: We discuss a many−body theory of the coherent ultrafast nonlinear optical response of systems with a strongly correlated electronic ground state that responds unadiabatically to photoexcitation. We introduce a truncation of quantum kinetic density matrix equations of motion that does not rely on an expansion in terms of the interactions and thus applies to strongly correlated systems. For this we expand in terms of the optical field, separate out contributions to the time−evolved many−body state due to correlated and uncorrelated multiple optical transitions, and use "Hubbard operator" density matrices to describe the exact dynamics of the individual contributions within a subspace of strongly coupled states, including "pure dephasing". Our purpose is to develop a quantum mechanical tool capable of exploring how, by coherently photoexciting selected modes, one can trigger nonlinear dynamics of strongly coupled degrees of freedom. Such dynamics could lead to photoinduced phase transitions. We apply our theory to the nonlinear response of a two−dimensional electron gas (2DEG) in a magnetic field. We coherently photoexcite the two lowest Landau level (LL) excitations using three time−delayed optical pulses. We identify some striking temporal and spectral features due to dynamical coupling of the two LLs facilitated by inter−Landau−level magnetoplasmon and magnetoroton excitations and compare to three−pulse four−wave−mixing (FWM) experiments. We show that these features depend sensitively on the dynamics of four−particle correlations between an electron−hole pair and a magnetoplasmon/magnetoroton, reminiscent of exciton−exciton correlations in undoped semiconductors. Our results shed light into unexplored coherent dynamics and relaxation of the quantum Hall system (QHS) and can provide new insight into non−equilibrium co−operative phenomena in strongly correlated systems.

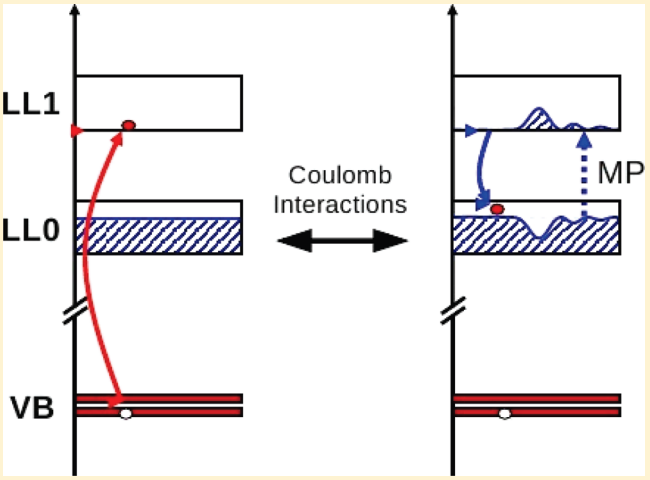

INTRODUCTION

The idea of controlling the properties of materials at the quantum level by using femtosecond laser pulses has led to promising developments at the frontier of condensed-matter physics and quantum chemistry.[1−6] This approach to materials science goes beyond traditional investigations of optical properties and focuses, for example, on the design of fast devices with a functional role in information storage and processing, memories, network components, etc. However, the development of these types of applications poses fundamental nonequilibrium physics questions, especially when subpicosecond device operation is desired. Advances in this important technological field will be greatly accelerated by a comprehensive description of transient cooperative phenomena and light−induced nonequilibrium phase transitions in condensed matter systems with strongly correlated electronic states. The development of quantum mechanical models able to treat light−induced dynamics of strongly coupled degrees of freedom is a serious challenge. It belongs to an emerging interdisciplinary field that brings together condensed matter, optical, and applied physics.

This paper outlines a systematic approach to the study of many-body systems with correlated electrons coherently coupled to light. We study nonequilibrium properties dominated by interactions among elementary excitations. While thermodynamic, transport, and linear optical properties do not depend as critically on such quasi-particle interactions, these dominate the nonlinear response to

Special Issue: Shaul Mukamel Festschrift

Received: December 14, 2010
Accepted: January 21, 2011
Published: March 11, 2011

external stimuli. Accepted rules of condensed matter physics, including the cornerstone concept of free energy, fail to describe the time evolution during femtosecond time scales. Our non-equilibrium many-body theory addresses all four of the following fundamental questions: How to describe the coherent photoexcitation of systems with strongly correlated ground state electrons reacting un-adiabatically to light? What is the nonlinear response to such photoexcitation? What detection scheme can best "visualize" this response? What many-body mechanisms are involved in the coherent and nonthermal temporal regimes?

During the last two decades, a good understanding of the ultrafast nonlinear optical response of undoped semiconductors has been achieved. Compared to multi-level atomic systems, the main theoretical challenge here is the description of interactions and correlations among exciton quasiparticles.[1,7,8] For this purpose, non-equilibrium theories such as the semiconductor Bloch equations,[2,5] dynamics controlled truncation scheme (DCTS),[9−11] correlation expansion,[8] Keldysh Green's functions,[2,5] correlation functions,[6] and canonical transformation "dressed semiconductor" approach[12] have been developed. In undoped semiconductors, one need not take into account correlations involving ground state electrons. A rigid Hartree−Fock ground state, with full valence bands and empty conduction band, suffices since Auger processes are negligible. However, when the conduction band is partly filled with N_e electrons in the ground state, low energy intraband electronic excitations can interact with the photoexcited carriers. If the fundamental reaction time of the ground state system to such interactions (determined by the period of one oscillation of the lowest excited state and by collective effects among the N_e electrons) is sufficiently long, it responds unadiabatically to the photoexcitation and thus cannot be treated as a "bath". The ultrafast nonlinear response is then strongly influenced by the quantum dynamics of the coupled system of photoexcited and ground state carriers. The theories describing the nonlinear response of undoped semiconductors must be extended to describe such effects.[12−16] For example, the DCTS truncates the hierarchy of density matrices generated by the interactions based on the assumption that all Coulomb interactions occur between photoexcited e−h pairs. The standard diagrammatic expansions and DCTS factorizations assume a Hartree−Fock reference state and no free ground state carriers. They break down in the case of a strongly correlated electronic ground state.

Photoinduced phase transitions in strongly correlated systems have attracted much attention recently, due to ultrafast switching applications and fundamental physics questions.[17,18] A prominent example of strong correlations between spin, charge, and orbital/lattice degrees of freedom is the colossal magneto-resistance observed in the $R_{1-x}A_xMnO_3$ Manganite materials (R = La, Pr, Nd, Sm, ... and A = Ca, Ba, Sr, Pd, ...).[18] Of particular interest here are macroscopic changes in the electronic states induced by perturbing strongly coupled degrees of freedom after the coherent excitation of selected modes.

The quantum Hall system (QHS) is another example of a well-characterized strongly correlated system. Here, a two−dimensional electron gas (2DEG) is subjected to a perpendicular magnetic field. The quantum well confinement and magnetic field quasi-confinement discretize the energy eigenstates into Landau levels (LL) with degeneracy $N = L^2/2\pi\ell^2$, where L is the system size and ℓ is the magnetic length. In the ground state, these LLs are partially filled with the correlated 2DEG.[19−21] The ratio of occupied states to LL degeneracy defines the filling factor $\nu = N_e/N = 2\pi\ell^2 n_e$, where N_e (n_e) denotes the number (density) of conduction electrons that populate the ground state. The LL degeneracy N increases with magnetic field and above a threshold value, $\nu \leq 2$, the ground state electrons only occupy the lowest LL (LL0) states; all of the higher LLs (LL1, ...) are then empty in the ground state. The coupling of the degenerate LL0 states by the Coulomb interaction results in a strongly correlated incompressible quantum liquid,[22] whose collective charge excitations are magnetoplasmons (MP) and magnetorotons (MR),[19−21,23−26] excitons of composite fermions,[27−29] interband quasiexcitons,[30] etc.

The QHS displays different correlated ground states depending on ν. At $\nu = 1$, the ground state becomes a ferromagnet with 100% spin polarization when the characteristic Coulomb energy exceeds the LL disorder broadening.[31] For weak disorder, the ground state around $\nu = 1$ includes a small population ($\propto|\nu - 1|$) of topologically charged spin texture quasiparticles (skyrmions).[31−35] For larger disorder, the ground state is maximally spin-polarized, however the empty states with respect to the $\nu = 1$ ferromagnetic state are populated by conventional Laughlin quasiparticles. At fractional ν, the e−e interaction removes the degeneracy of the noninteracting system and produces robust ground states, separated from the excited states by an energy gap (incompressibility). This nonperturbative effect can be interpreted by considering the formation of composite fermion quasiparticles, i.e., topological bound states of an electron and an even number of magnetic flux quantized vortices.[28,29] The strongly interacting electrons are transformed into weakly interacting composite fermions and the partly filled lowest electron LL splits into several composite fermion LLs. Fractional quantum Hall effects occur when an integer number of composite fermion LLs are fully occupied.[28,29] In terms of applications, the quantum coherence of the QHS may be useful for realizing robust many-body qubits that can be coherently controlled with light for implementing quantum computation schemes.[36] Ultrarafast nonlinear spectroscopy can shed light into the coherent dynamics of the QHS.[37−46] The above developments make our theoretical advances, which address transient coherence and relaxation in strongly correlated systems, particularly timely.

In the first part of this paper, we obtain the third-order nonlinear optical response by considering a hierarchy of quantum kinetic density matrix equations of motion. In the QH and other strongly correlated systems, there is no small interaction parameter that could be used to truncate this hierarchy. We consider a system that satisfies the following conditions: (i) an expansion in terms of the optical field is appropriate, (ii) the optical response is determined by electronic transitions between two (or more) "bands", i.e., separate manifolds of many-body states that are disconnected in the absence of photoexcitation, and (iii) the optical transitions occur between a full valence band and a partially filled conduction band. We treat nonlinear intraband and interband density matrices by expanding in terms of the optical field and noting that, similar to the DCTS,[11] there is a one to one correspondence between number of valence holes and number of emitted/absorbed photons. This correspondence allows us to separately treat the dynamics within a subspace of many-body states with fixed (small) number of holes and many electrons. For this we expand in terms of "Hubbard operators" of the form $|n\rangle\langle m|$, where $|n\rangle$ is a finite basis of many−body states that spans the relevant subspace, and then solve nonperturbatively a closed system of equations of motion for the density matrices $\langle|n\rangle\langle m|\rangle$ including relaxation. Similar equations of motion were introduced by Hubbard to treat strong local correlations.[47] They

dx.doi.org/10.1021/jp1118794 |J. Phys. Chem. B 2011, 115, 5634–5647

have since been used to study e.g. the Hubbard Hamiltonian,[48] spin excitations in the manganites,[49] X−X correlations in undoped semiconductors,[50] and density matrices in Liouville space.[3] In the undoped system, $N_e = 0$ and all carriers come from photoexcited e−h pairs. As a result, the relevant subpaces are spanned by 1−h+1−e and 2−h+2−e states, which reduces the number of independent density matrices.[9−11]

Our theory proceeds in three steps. First, we obtain the linear interband coherent amplitudes (e.g., the optical polarization) by calculating the time−evolution within a subspace of $1-h+-(N_e+1)-e$ states. This first step addresses the interactions of a photoexcited $e-h$ pair with the ground state electrons, which can strongly perturb the ground state. In the QHS, such interactions can lead, for example, to the formation of trion bound states or quasiexcitons.[30,51−55] As a second step, we study the second−order response, determined by dynamics of carrier populations and light−induced coherent (Raman) couplings between different many−body states with fixed number of carriers. We introduce "pure dephasing"[3] that does not allow the corresponding intraband density matrices to be expressed as products of interband coherent amplitudes, as in the case of a wave function approach (coherent limit). This is important since experiments indicate strong deviations from the coherent limit. Finally, we consider the third−order response, which depends on the dynamics within the $2-h+(N_e+2)-e$ subspace. Given the complexity of describing this dynamics, we introduce a decomposition of the time-evolved many−body wave function into correlated and uncorrelated parts, analogous to the cumulant expansions of the DCTS, which however also applies to systems with a populated correlated ground state. This decomposition allows us to separate the contributions to the third−order density matrices that can be expressed as products of optical polarizations from the fully correlated (irreducible) contributions, whose dynamics is determined by memory effects due to multi−particle correlations.[1,7,10,56] In the second part of the paper, we compare the predictions of our theory with femtosecond three-pulse four-wave mixing (FWM) experiments. We show that the coupling between {1-LL0-e + 1-LL1-h + LL0→LL1MP} four-particle correlations and magnetoexcitons determines the spectral and temporal profile of the QHS FWM signal. The latter depends sensitively on the dephasing of the above four−particle correlations and the coupling of magnetoroton 2DEG excitations. We identify the experimental signatures of such effects, which can be controlled, e.g., by tuning the photoexcitation frequency.

MANY-BODY THEORY OF THE OPTICAL RESPONSE

In this section we formulate the optical response of a system described by the general Hamiltonian

$$H = \sum_{\alpha}(E_g + \varepsilon_\alpha^c)\hat{e}_\alpha^\dagger\hat{e}_\alpha + \sum_{\alpha}\varepsilon_\alpha^v\hat{h}_\alpha^\dagger\hat{h}_\alpha + H_{\text{int}} \qquad (1)$$

where we assume two bands well-separated in energy by E_g: a "conduction band" (partially filled in the ground state) and a "valence band" (full in the ground state). The operators $\hat{e}_\alpha^\dagger$ ($\hat{h}_\alpha^\dagger$) create a conduction (valence) electron (hole) state labeled by a composite index α that contains all relevant single-particle quantum numbers. $\varepsilon_\alpha^{e,h}$ are the corresponding energies, determined by the bandstructure (e.g., Kohn−Sham orbitals).[57] H_{int} describes e−e, e−h, h−h, or other interactions, which we assume do not couple the two bands. For example, in the manganites one may consider different orbital states and orbiton or other excitations between them and include Hubbard and Jahn−Teller interactions in H_{int}.[18,49] In semiconductors, the Hamiltonian is discussed, for example, in refs 2, 5, and 11. In J-aggregate and organic systems, H can be expressed in terms of Frenkel exciton operators (Paulions) and their interactions.[3,6,11]

Within the dipole approximation,[5] the light-matter system is described by the Hamiltonian

$$H(t) = H - [d(t)\hat{X}^\dagger + \text{h.c.}] \qquad (2)$$

where $d(t) = \mu E(t)$ is the Rabi energy. We consider optical transitions between the e and h bands. μ is the interband transition matrix element, determined by the bandstructure, and $\hat{X}^\dagger$ is the interband transition operator, expressed as a linear combination of e−h pair creation operators $\hat{e}_\alpha^\dagger\hat{h}_\beta^\dagger$. Since N_e electrons populate the conduction band prior to photoexcitation, when following the effects of the applied optical fields we count the number of valence band holes in a given many-body state. Therefore, we use the shorthand notation 0−h, 1−h, 2−h ,... to label the states. We assume for simplicity zero temparature, in which case the system initially occupies the $0-h+N_e-e$ ground state $|G\rangle$ of the Hamiltonian H. However, our results can be extended to a mixed initial state with finite temperature. We express the state that evolves from $|G\rangle$ according to the Hamiltonian $H(t)$ as $|\psi\rangle = |\psi_0\rangle + |\psi_1\rangle + |\psi_2\rangle$, where $|\psi_n\rangle$ is the projection to the $n-h+(N_e+n)-e$ subspace.[15,44] States with $n \geq 3$ valence holes do not contribute to the third-order nonlinear polarization when the Hamiltonian H conserves the number of holes. Such a decomposition can be performed in any system where distinct manifolds of many-body states are only connected dynamically by light.

First-Order Optical Response: Interband Polarization. In this section we obtain the density matrix $\langle\hat{Z}\rangle$ to $O(E)$ for any operator $\hat{Z}$ that decreases the number of h's by one (interband operator). Noting that the Hamiltonian H conserves the number of h's, while in the ground state the valence band is full, the $O(E)$ contribution to such density matrices comes from the dynamics within the subspace of $1-h+(N_e+1)-e$ many-body states. We denote by $|\psi_{1L}(t)\rangle$ the $O(E)$ 1−h contribution to the many-body state that evolves in time from the correlated ground state $|G\rangle$ according to the Hamiltonian eq 2.[15,44] To $O(E)$

$$\langle\hat{Z}\rangle^L = \langle G|\hat{Z}|\psi_{1L}(t)\rangle = \langle|G\rangle\langle G|\hat{Z}\rangle^L \qquad (3)$$

which coincides with the density matrix of the "Hubbard operator" $|G\rangle\langle G|\hat{Z}$.[47,50] By expanding the state $\hat{Z}^\dagger|G\rangle$ in terms of a basis $|n\rangle$ that spans the $1-h+(N_e+1)-e$ subspace of interest, we can then reduce the calculation of any $\langle\hat{Z}\rangle^L$ to a closed system of equations of motion for the density matrices $\langle|G\rangle\langle n|\rangle^L$. These equations describe the exact dynamics within the given subspace.

To treat this dynamics, we consider an orthonormal set of $1-h+(N_e+1)-e$ states $|X_i\rangle$ and $|Y_\alpha\rangle$, where $\langle X_i|\hat{X}^\dagger|G\rangle \neq 0$ ("bright" configurations) and $\langle Y_\alpha|\hat{X}^\dagger|G\rangle = 0$ ("dark" configurations). We expand any $\langle\hat{Z}\rangle^L$ in terms of the linearized density matrices

$$P_i^L = \frac{\langle|G\rangle\langle X_i|\rangle^L}{\sqrt{N}},\ \bar{P}_\alpha^L = \frac{\langle|G\rangle\langle Y_\alpha|\rangle^L}{\sqrt{N}} \qquad (4)$$

where N is proportional to the system size. In the absence of an expansion parameter for treating the interactions, we must describe the exact dynamics within the subspace spanned by the above states, whose choice depends on the system and filling

factor of interest. Defining the energies

$$\Omega_i = \langle X_i|H|X_i\rangle, \quad \overline{\Omega}_\alpha = \langle Y_\alpha|H|Y_\alpha\rangle \tag{5}$$

and the interaction parameters

$$V_{ij} = -\langle X_i|H|X_j\rangle, \quad W_{\alpha\alpha'} = N\langle Y_\alpha|H|Y_{\alpha'}\rangle,$$
$$W_{\alpha i} = \sqrt{N}\langle Y_\alpha|H|X_i\rangle \tag{6}$$

we obtain the following closed system of equations of motion, exact within the subspace of interest

$$i\partial_t P_i^{\mathrm{L}} = (\Omega_i - i\Gamma_i)P_i^{\mathrm{L}} - \sum_{j\neq i} V_{ij}P_j^{\mathrm{L}} - \frac{d(t)}{\sqrt{N}}\langle X_i|\hat{X}^\dagger|G\rangle + \frac{1}{\sqrt{N}}\sum_\alpha W_{i\alpha}\overline{P}_\alpha^{\mathrm{L}} \tag{7}$$

where we introduced the dephasing rates Γ_i absent in a wave function approach, and

$$i\partial_t \overline{P}_\alpha^{\mathrm{L}} = (\overline{\Omega}_\alpha - i\gamma_\alpha)\overline{P}_\alpha^{\mathrm{L}} + \frac{1}{\sqrt{N}}\sum_i W_{\alpha i}P_i^{\mathrm{L}} + \frac{1}{N}\sum_{\alpha'\neq\alpha} W_{\alpha\alpha'}\overline{P}_{\alpha'}^{\mathrm{L}} \tag{8}$$

where we introduced the dephasing rates γ_α. If $|X_i\rangle$ were exact many-body eigenstates of H, $W_{\alpha i} = V_{ij} = 0$ and the above equations of motion decouple. However, this requires an accurate calculation of all excited many−body eigenstates. Any basis of 1−h+(N_e+1)−e states that spans the subspace of interest can however be used to calculate the above density matrices directly in the time domain, including dephasing. When the dephasing rates γ_α and Γ_i become comparable to the characteristic interaction energies, they can play an important role in the optical dynamics.

We now discuss some specific examples of states $|X_i\rangle$ and $|Y_\alpha\rangle$. First we make the connection to the case of exciton−phonon interactions,[11] in semiconductors[8,10] or in J aggregrates and organic crystals.[3,6] In this case, we can distinguish between "system" and "bath" and choose $|X_i\rangle$ as (bound or unbound) e−h pair or Frenkel exciton states and $|Y_\alpha\rangle$ as exciton+phonon (or vibronic) states. Equations 7 and 8 then describe non-Markovian dephasing and polaronic effects due to noninstantaneous exciton−phonon interactions, while the last term on the right-hand side (rhs) of eq 8 describes vertex corrections beyond the perturbative Born approximation of the system−bath interaction. The Markovian and dephasing rate approximations of instantaneous interactions with the bath are recovered by solving eq 8 within the adiabatic and Born approximations.[8,11]

In a purely electronic system, however, one cannot clearly distinguish the system from the "bath". Nevertheless, one could still view the excitations of the ground state electrons as analogous to the phonons discussed above and consider, for example, configurations $|X_i\rangle$ of the form $\hat{e}^\dagger\hat{h}^\dagger|G\rangle$ and configurations $|Y_\alpha\rangle$ of the form $\hat{e}^\dagger\hat{h}^\dagger\hat{e}^\dagger\hat{e}|G\rangle$. Such Y_α states describe the coupling between exciton and electronic excitations such as, e.g., magnetoplasmons or magnetorotons in the QHS[16] and orbital or other charge excitations in the manganites.[18,47,49] The unadiabatic response of a strongly correlated N_e−electron ground state to such couplings can lead to non-Markovian dynamics. For example, an incompressible Laughlin quantum liquid has an excitation energy gap determined by the electron−electron interactions.[22] Its dynamical response is governed by Laughlin[22] and composite fermion[28,29] correlations. The photoexcited e−h pair can also bind ground state electrons and form trion or higher complexes, which are Laughlin-correlated with the rest of the electrons. Such effects manifest themselves as extra peaks in the optical spectra of the QH or 2DEG systems.[30,51−55,61] For $N_e = 1$, with ground state $|G\rangle = \hat{e}_0^\dagger|0\rangle$ ($|0\rangle$ denotes full valence−empty conduction band), we can choose $|X_i\rangle = \hat{e}_\alpha^\dagger\hat{h}_\beta^\dagger\hat{e}_0^\dagger|0\rangle = \hat{e}_\alpha^\dagger\hat{h}_\beta^\dagger|G\rangle$ and $|Y_\alpha\rangle = \hat{e}_\alpha^\dagger\hat{h}_\beta^\dagger\hat{e}_\gamma^\dagger|0\rangle = \hat{e}_\alpha^\dagger\hat{h}_\beta^\dagger\hat{e}_\gamma^\dagger\hat{e}_0|G\rangle$, where $\alpha,\gamma \neq 0$. In the QHS, calculations of quasiexciton[30] and trion[55] contributions to the photoluminescence at fractional ν were based on exact diagonalizations of H for small N_e, using a basis of 1−h+(N_e+1)−e Slater determinants.[30,55] Exact diagonalizations of small systems describe well ground state and excitation properties of the QHS.[19,30,55] Another example of a convenient basis for treating time−dependence is the Lanczos basis.[15,60]

Second-Order Response: Populations and Intraband Many-Body Coherences. In this section we describe the $O(E^2)$ contribution to any intra−band density matrix $\langle\hat{M}\rangle$, where $\hat{M}$ conserves the number of holes. Examples of such density matrices are the carrier populations and intraband coherences between many−body states with the same number of electrons and holes. We first note that the 2−h contribution to $\langle\hat{M}\rangle$ is $O(E^4)$. Within the 1−h subspace, $\langle\hat{M}\rangle$ can be expanded in terms of the "Hubbard operator" density matrices $\langle|X_i\rangle\langle X_j|\rangle$, $\langle|X_i\rangle\langle Y_\alpha|\rangle$, and $\langle|Y_\alpha\rangle\langle Y_{\alpha'}|\rangle$. In a wave function approach, these density matrices can be expressed as products of the interband amplitudes P_i^{L} and $\overline{P}_\alpha^{\mathrm{L}}$. However, "pure dephasing"[3] processes introduce additional intraband dynamics, described by the nonfactorizable contributions

$$N_{ij} = \frac{1}{N}\langle|X_i\rangle\langle X_j|\rangle - P_j^{\mathrm{L}}P_i^{\mathrm{L}*},$$
$$M_{j\alpha} = \frac{1}{N}\langle|X_j\rangle\langle Y_\alpha|\rangle - P_j^{\mathrm{L}*}\overline{P}_\alpha^{\mathrm{L}},$$
$$N_{\alpha\alpha'} = \frac{1}{N}\langle|Y_\alpha\rangle\langle Y_{\alpha'}|\rangle - \overline{P}_\alpha^{\mathrm{L}*}\overline{P}_{\alpha'}^{\mathrm{L}} \tag{9}$$

In the absence of a small interaction parameter, one must describe the full intraband dynamics within the subspace of 1−h+(N_e+1)−e many−body states, by solving the closed system of $O(E^2)$ equations of motion below. The dynamical coupling between $|X_i\rangle$ and $|X_j\rangle$ is described by[16]

$$i\partial_t N_{ij} = (\Omega_j - \Omega_i - i\Gamma_{ij})N_{ij} + i(\Gamma_i + \Gamma_j - \Gamma_{ij})P_j^{\mathrm{L}}P_i^{\mathrm{L}*} + \sum_{i'\neq i} V_{i'i}N_{i'j} - \sum_{j'\neq j} V_{jj'}N_{ij'} + \frac{1}{\sqrt{N}}\sum_\alpha (W_{\alpha j}^* M_{i\alpha} - W_{\alpha i}M_{j\alpha}^*) \tag{10}$$

where the first line on the rhs comes from the difference between intraband and interband dephasing rates ("pure dephasing"[3]) and the second line comes from the interaction-induced couplings. The latter are strong between almost degenerate many-body states within our subspace, similar, e.g., to the nonperturbative quantum Hall effects.[19,20,22]

$$i\partial_t M_{i\alpha} = (\overline{\Omega}_\alpha - \Omega_i - i\Gamma_{i\alpha})M_{i\alpha} + i(\Gamma_i + \gamma_\alpha - \Gamma_{i\alpha})P_i^{\mathrm{L}*}\overline{P}_\alpha^{\mathrm{L}} + \frac{1}{\sqrt{N}}\sum_{i'} W_{\alpha i'}N_{ii'} - \frac{1}{\sqrt{N}}\sum_{\alpha'} W_{\alpha' i}N_{\alpha'\alpha} + \sum_{i'\neq n} V_{i'i}M_{i'\alpha} + \frac{1}{N}\sum_{\alpha'\neq\alpha} W_{\alpha\alpha'}M_{i\alpha'} \tag{11}$$

describes the coherent second-order light-induced coupling between the $|X_i\rangle$ and $|Y_\alpha\rangle$ states, and

$$i\partial_t N_{\alpha\alpha'} = (\overline{\Omega}_{\alpha'} - \overline{\Omega}_{\alpha} - i\Gamma_{\alpha\alpha'})N_{\alpha\alpha'} + i(\gamma_\alpha + \gamma_{\alpha'} - \Gamma_{\alpha\alpha'})\overline{P}^{L*}_{\alpha}\overline{P}^{L}_{\alpha'} + \frac{1}{\sqrt{N}}\sum_i (W_{\alpha' i}M^*_{i\alpha} - W^*_{\alpha i}M_{i\alpha'}) + \frac{1}{N}\sum_{\alpha''\neq\alpha'} W^*_{\alpha''\alpha'}N_{\alpha\alpha''} - \frac{1}{N}\sum_{\alpha''\neq\alpha} W_{\alpha''\alpha}N^*_{\alpha'\alpha''} \quad (12)$$

The interaction matrix elements and excitation energies entering in the above equations are the same as in the previous section. The above nonfactorizable density matrices vanish in the coherent limit $\Gamma_{ij} = \Gamma_i + \Gamma_j$, $\Gamma_{i\alpha} = \Gamma_i + \gamma_\alpha$, and $\Gamma_{\alpha\alpha'} = \gamma_\alpha + \gamma_{\alpha'}$. As observed experimentally, deviations from this limit are strong and result in long−lived incoherent populations and intraband coherences.

Third-Order Nonlinear Polarization. In this section we obtain directly the third-order nonlinear polarization that determines the ultrafast nonlinear optical spectra. Generally, we can express the optical transition operator $\hat{X}$ as

$$\hat{X}^\dagger = \sqrt{N}\sum_n \hat{X}^\dagger_n \quad (13)$$

where $\hat{X}^\dagger_n$ are linear combinations of e−h pair creation operators $\hat{e}^\dagger_\alpha\hat{h}^\dagger_\beta$ that satisfy the optical transition selection rules (e.g., momentum or angular momentum conservation) and the symmetries of the system. For example, $\hat{X}^\dagger_n$ can be chosen to create exciton eigenstates in undoped semiconductors[50] or Frenkel excitons in organic systems.[3,6] We introduce the e−h "excitonic configurations" $|X_n\rangle = \hat{X}^\dagger_n|G\rangle$, with unexcited ground state, and assume orthogonality: $\langle X_n|X_m\rangle = (1 - \nu_n)\delta_{nm}$, where ν_n is determined by the ground state carrier population.[16] Within the dipole approximation, the optical response is described by the polarization (e−h coherence)[2,4]

$$P(t) = \mu\sum_n P_n(t), \quad P_n(t) = \frac{\langle\hat{X}_n\rangle}{\sqrt{N}} \quad (14)$$

where the nonlinear polarizations P_n are determined by their equations of motion. The interactions between X_n and the ground state thermal carriers[13,14,30] couple $|X_n\rangle$ to the excited configurations $|Y_n\rangle$, which are defined by the equation[15]

$$H|X_n\rangle = \Omega_n|X_n\rangle - (1-\nu_n)\sum_{m\neq n} V_{mn}|X_m\rangle + |Y_n\rangle \quad (15)$$

and the orthogonality requirement $\langle X_m|Y_n\rangle = 0$ (irreducibility condition). We obtain[16]

$$\Omega_n = \frac{\langle X_n|H|X_n\rangle}{\langle X_n|X_n\rangle}, \quad V_{nn'} = -\frac{\langle X_n|H|X_{n'}\rangle}{(1-\nu_n)(1-\nu_{n'})} \quad (16)$$

for any strongly correlated ground state and introduce the operator

$$\hat{Y}_n = [\hat{X}_n, H] - \Omega_n\hat{X}_n + (1-\nu_n)\sum_{n'\neq n} V_{nn'}\hat{X}_{n'} \quad (17)$$

The nonlinear polarization equation of motion then reads[16]

$$i\partial_t P_n(t) - \Omega_n P_n(t) + (1-\nu_n)\sum_{n'\neq n} V_{nn'}P_{n'}(t) = -d(t)[1-n_n(t)] + \frac{\langle\hat{Y}_n\rangle}{\sqrt{N}} \quad (18)$$

The first term on the rhs describes the PSF effects, determined by the total carrier population $n_n(t)$, and recovers the results of a multi−level atomic-like system if we set $V_{nn'} = 0$.[3] More generally, n_n also depends on intraband coherences $\langle\hat{e}^\dagger_\alpha\hat{e}_\beta\rangle$ and $\langle\hat{h}^\dagger_\alpha\hat{h}_\beta\rangle$, e.g., in the case of spin interaction effects in the nonlinear optical response of magnetic semiconductors.[58]

The second term on the rhs of eq 18, $\langle\hat{Y}_n\rangle$, describes deviations of the many−body system from a multi-level atomic-like system.[3] These deviations are due to the coupling of X_n with other degrees of freedom. For example, in the case of exciton−phonon interactions, $\langle\hat{Y}_n\rangle$ describes phonon−assisted density matrices.[10,11] In the case of Coulomb interactions, $\langle\hat{Y}_n\rangle$ can be expanded in terms of density matrices of the form $\langle\hat{e}^\dagger\hat{e}\hat{e}\hat{h}\rangle$ and $\langle\hat{h}^\dagger\hat{h}\hat{e}\hat{h}\rangle$, which describe the interaction of an e−h pair with an electronic excitation. The factorization of these density matrices gives the Semiconductor Bloch equations.[2,5] However, this Hartree−Fock treatment of the interactions misses e.g. biexciton, trion, and exciton-2DEG inelastic scattering effects. In the undoped system, where the conduction band is empty and the valence band is full, $\langle\hat{Y}_n\rangle$ describes the interactions of X_n with other photoexcited carriers or phonons. In the case of a populated ground state, there are additional X_n interactions with the thermal electrons, which are described by the action of operators of the form $\hat{e}^\dagger\hat{h}^\dagger\hat{e}^\dagger\hat{e}$ on the 0−h+N_e−e subspace of states. The calculation of $\langle\hat{Y}_n\rangle$ is the purpose of this section. More generally however, we obtain below an expression of $\langle\hat{Z}\rangle$ for any interband operator $\hat{Z}$ that reduces the number of holes by one.

The nonlinear response arises from multiple optical transitions and corresponding e−h pair creation/annihilation processes. During each single-photon transition, the photoexcited e−h pair interacts with the ground state electrons as described by P^L_n. We want to separate out all contributions to the nonlinear density matrix that can be expressed in terms of products of one or more of the coherent amplitudes P^L_n measured in linear absorption. The remaining contributions are then determined by time integrals of P^L_n with memory kernels due to multi-excitation correlations. We use the following decomposition, which separates the n−h subspaces coupled only by the light:

$$\langle\hat{Z}\rangle = \langle\psi_0|\hat{Z}|\psi_1\rangle + \langle\psi_{1L}|\hat{Z}|\psi_2\rangle + O(E^5) \quad (19)$$

We then separate the contributions of correlated or uncorrelated multiple optical transitions by first identifying the parts of $|\psi_n\rangle$ whose amplitudes can be expressed in terms of products of P^L_n. Such factorizable contributions assume that, although the photoexcited quasiparticles are strongly correlated with the ground state electrons, their interactions with each other can be treated in a mean field fashion. In the undoped system, the DCTS cumulant expansions serve a similar purpose.[9−11] Here we accomplish this for a strongly correlated populated ground state, where Wick's theorem does not apply, and recover the DCTS in the undoped system. Importantly, our decomposition allows us to obtain a closed system of equations of motion by projecting each contribution to the appropriate subspace of states with fixed number of h's. For example, in the undoped

system, the number of independent density matrices is reduced in this way since we can project to subspaces spanned by X or X + X states.

First we consider the time-evolved 1−h state $|\psi_{1L}\rangle$ and separate the coherent contributions P_n^L by projecting the $|X_n\rangle$ states:

$$|\psi_{1L}\rangle = \sum_n \frac{\langle \hat{X}_n\rangle^L}{1-\nu_n}|X_n\rangle + |\overline{\psi}_{1L}\rangle \tag{20}$$

where $\langle X_n|\bar{\psi}_{1L}\rangle = 0$. Thus, $|\bar{\psi}_{1L}\rangle$ does not contribute to the linear absorption, which is determined by $\langle \hat{X}_n\rangle^L$. It is obtained from the equation of motion[15]

$$i\partial_t|\overline{\psi}_{1L}\rangle = H|\overline{\psi}_{1L}\rangle + \sum_n \frac{\langle \hat{X}_n\rangle^L}{1-\nu_n}|Y_n\rangle - \sum_n \frac{\langle \hat{Y}_n\rangle^L}{1-\nu_n}|X_n\rangle \tag{21}$$

and involves time integrals of the linear polarizations with a memory kernel determined by correlations between X_n and ground state (thermal) electrons. The nontrivial problem in solving this equation is how to describe the strong interaction of the valence hole with the $N_e + 1$ electrons. In the case of the Fermi Edge Singularity, this was accomplished by considering a time-dependent coupled cluster expansion expression for $|\bar{\psi}_{1L}\rangle$, which describes an exciton dressed by a macroscopic number of Fermi sea pairs.[13] A cluster expansion can also be considered in the case of phonons.[3] Equation 21 can be solved by projecting the basis states $|X_i\rangle$ and $|Y_\alpha\rangle$ discussed above.

Next we turn to the two-photon processes that excite two e−h pairs on top of the N_e ground state electrons. Such 2−h+(N_e+2)−e configurations are determined by the equation of motion

$$i\partial_t|\psi_2\rangle = H|\psi_2\rangle - d(t)\hat{X}^\dagger|\psi_{1L}\rangle + O(E^4) \tag{22}$$

$|\psi_2\rangle$ can be described by introducing a basis of 2−h+(N_e+2)−e states.[59] Given the complexity of treating such states, however, we consider the following exact decomposition of $|\psi_2\rangle$ into an uncorrelated part, which assumes that each photoexcited e−h pair interacts independently with the ground state electrons, and a part that describes correlations among the two optical transitions

$$|\psi_2\rangle = \frac{1}{2}\sum_{nm}\frac{\langle \hat{X}_n\rangle^L\langle \hat{X}_m\rangle^L}{(1-\nu_n)(1-\nu_m)}\hat{X}_n^\dagger\hat{X}_m^\dagger|G\rangle + \sum_n \frac{\langle \hat{X}_n\rangle^L}{1-\nu_n}\hat{X}_n^\dagger|\overline{\psi}_{1L}\rangle + |\overline{\psi}_2\rangle + O(E^4) \tag{23}$$

The first two term on the rhs come from two uncorrelated optical transitions. The correlated contribution $|\bar{\psi}_2\rangle$ is determined by the equation of motion

$$i\partial_t|\overline{\psi}_2\rangle - H|\overline{\psi}_2\rangle = \frac{1}{2}\sum_{nm}\langle \hat{X}_n\rangle^L\langle \hat{X}_m\rangle^L[\hat{Y}_n^\dagger, \hat{X}_m^\dagger]|G\rangle + \sum_n[\langle \hat{X}_n\rangle^L\hat{Y}_n^\dagger - \langle \hat{Y}_n\rangle^L\hat{X}_n^\dagger]|\overline{\psi}_{1L}\rangle \tag{24}$$

where the first term on the rhs describes a correlated four-particle excitation, analogous to the undoped system,[1,56] which interacts with the ground state electrons. $|\bar{\psi}_2\rangle$ leads to density matrix contributions determined by time integrals of the polarizations with a memory kernel and can be obtained by projecting to a subspace of 2−h+(N_e+2)−e states.[59] In the same way, we decompose the 0−h state $|\psi_0\rangle$, created by two−photon Raman processes of excitation and then deexcitation of an e−h pair, as

$$|\Psi_0\rangle = \langle G|\Psi\rangle|G\rangle - \sum_n \frac{\langle \hat{X}_n\rangle^{L^*}}{1-\nu_n}\hat{X}_n|\overline{\Psi}_{1L}\rangle + |\overline{\Psi}_0\rangle + O(E^4) \tag{25}$$

where $\langle G|\bar{\psi}_0\rangle = 0$. By substituting the above decompositions to eq 19 we obtain[15,16,44]

$$\langle \hat{Z}\rangle = \sum_n \frac{\langle \hat{X}_n\rangle^{L^*}}{1-\nu_n}\langle G|[\hat{X}_n, \hat{Z}]|\psi_2\rangle + \sum_n \frac{\langle \hat{X}_n\rangle^L}{1-\nu_n}\langle [\hat{Z}, \hat{X}_n^\dagger]\rangle_c + \langle \hat{Z}\rangle_{corr} + \frac{1}{2}\sum_{nn'}\frac{\langle \hat{X}_n\rangle^L\langle \hat{X}_{n'}\rangle^L}{(1-\nu_n)(1-\nu_{n'})}\langle \overline{\psi}_{1L}|[[\hat{Z}, \hat{X}_n^\dagger], \hat{X}_{n'}^\dagger]|G\rangle + \langle \overline{\psi}_{1L}|\hat{Z}|\overline{\psi}_2\rangle + \langle \overline{\psi}_0|\hat{Z}|\overline{\psi}_{1L}\rangle \tag{26}$$

where we introduced the irreducible intraband density matrix

$$\langle [\hat{Z}, \hat{X}_n^\dagger]\rangle_c = \langle [\hat{Z}, \hat{X}_n^\dagger]\rangle - \sum_{n'm'}\frac{\langle \hat{X}_{n'}\rangle^{L^*}\langle \hat{X}_{m'}\rangle^L}{(1-\nu_{n'})(1-\nu_{m'})}\langle X_{n'}|[\hat{Z}, \hat{X}_n^\dagger]|X_{m'}\rangle - \sum_{n'}\frac{\langle \hat{X}_{n'}\rangle^{L^*}}{1-\nu_{n'}}\langle G|[\hat{X}_{n'}, [\hat{Z}, \hat{X}_n^\dagger]]|\overline{\psi}_{1L}\rangle - \sum_{n'}\frac{\langle \hat{X}_{n'}\rangle^L}{1-\nu_{n'}}\langle \overline{\psi}_{1L}|[[\hat{Z}, \hat{X}_n^\dagger], \hat{X}_{n'}^\dagger]|G\rangle \tag{27}$$

In the undoped system, the above density matrix describes incoherent populations and $X \leftrightarrow X$ coherences or coherent phonon effects.[10,11]

$$\langle \hat{Z}\rangle_{corr} = \langle |G\rangle\langle Z|\rangle + \sum_n \frac{\langle \hat{X}_n\rangle^{L^*}}{1-\nu_n}\langle Z|\hat{X}_n|\psi_2\rangle - \frac{\langle \hat{X}_n\rangle^L}{1-\nu_n}\langle Z|X_n^\dagger|\overline{\psi}_0\rangle \tag{28}$$

is determined by the dynamics of the 1−h+(N_e+1)−e excitation $|Z\rangle = \hat{Z}^\dagger|G\rangle$ and the nonlinear density matrix $\langle |G\rangle\langle Z|\rangle$, similar to the linear response. It can thus be calculated by solving a closed system of equations of motion, obtained by expanding $|Z\rangle$ in terms of $|X_i\rangle$ and $|Y_\alpha\rangle$ similar to the linear polarization calculation. $\langle \hat{Y}_n\rangle_{corr}$ describes the dynamical response of the correlated ground state to the photoexcited e−h pair due to X_n-ground state electron interactions. It includes trion[51] and quasi−exciton[30] nonlinearities and vanishes in the undoped system. It also describes the phonon−assisted polaronic effects in a way analogous to the linear polarization calculation.

An advantage of using eq 26, rather than trying to solve the equation of motion of $\langle \hat{Z}\rangle$ directly, is that it allows us to separately treat the dynamics within each n−h+(N_e+n)−e subspace of many-body states. Another advantage is that it separates out processes that lead to distinct contributions to the multi-dimensional nonlinear spectra (e.g., dephasing vs relaxation). Equation 26 also separates the nonlinear terms whose dynamics is determined by P_n^L from those determined by integrals of P_n^L with memory kernels given by different correlations. For example, $\langle Z\rangle_{corr}$ and $|\bar{\psi}_{1L}\rangle$ depend on correlations between X_n and electronic excitations of the thermal electrons, $|\bar{\psi}_2\rangle$ depends on correlations between two Xs, and $\langle [\hat{Z}, \hat{X}_n^\dagger]\rangle_c$ depends on intraband coherent dynamics and relaxation. Finally, eq 26 allows us to treat the coherent ultrafast response of a strongly correlated system while maintaining the connection with the well-established results and intuition obtained in the well-understood undoped system.[10,11] We note, for example, that the first term on its rhs describes an X−X

interband coherence that recovers the treatment of X−X interactions in undoped semiconductors.[16,50,59] The decomposition of this X−X coherence into Hartree−Fock and correlated contributions[50,56,59] is obtained by using eq 23.

INTER-LL DYNAMICAL COUPLINGS IN THREE-PULSE FOUR-WAVE-MIXING

In this second part of the paper we corroborate, by comparing our microscopic calculation and experiment, our earlier claim that the dynamical coupling of the two lowest magnetoexcitons by inter-LL MP and MR excitations is an important nonlinearity in the QHS. For this we present numerical results obtained by calculating the parameters that enter the theory using the $\nu = 1$ QH ground state and a Hamiltonian that captures the essential physical processes.

Description of the Model. We consider a two-band Hamiltonian describing two-dimensional electrons and holes subject to a perpendicular magnetic field.[16] We also consider right-circularly polarized light, which excites a single interband transition that creates spin−↓ electrons and results in a single LL0 peak.[40] We use the Landau gauge and label the single-particle states by $\alpha = (k,n,\sigma)$, where k is proportional to the cyclotron orbit center x-coordinate, n is the LL index, and s denotes the carrier spin. $\varepsilon_\alpha^{e,h} = \omega_c^{e,h}(n+1/2)$, where $\omega_c^{e,h} = eB/m_{e,h}$ are the electron and hole cyclotron energies ($\hbar = 1$). Although this discrete LL energy structure resembles an atomic system, each level has a macroscopic degeneracy N. Some particularities of the realistic system missed by our model, such as finite quantum well height and width, symmetric vs asymmetric doping and confining potential profiles, spin−orbit interaction, etc lift the optical selection rules due to invariance under magnetic translations ("geometric symmetry")[61] and electron−hole symmetry ("hidden symmetry").[51,62,63] This is important, e.g., for trion formation and for the observation of skyrmion and composite fermion effects.[55] Nevertheless, our predicted spectral and temporal features, due to LL0−LL1 dynamical coupling, are ubiquitous and largely independent of such particularities.

At $\nu = 1$, the 2DEG in the ground state Laughlin wave function[22] populates all N of the spin−↑ LL0 states, while all spin−↓ LL0 states and all higher LLs are empty. Signatures of such spin polarization[20,64] were observed in linear absorption experiments at temperatures as high as a few Kelvin.[65] The lowest 2DEG neutral excitations are LL0 → LL1 excitations, while screening is suppressed by the LL0−LL1 energy gap.[24] Due to the hidden symmetry,[62] $\langle \hat{Y}_n \rangle$ in eq 18 vanishes if we project within a single LL, in which case the optical response resembles that of a noninteracting system. We break the hidden symmetry by photoexciting both LL0 and LL1 states and by considering LL0−LL1 mixing due to inter-LL 2DEG excitations. We neglect states with energy comparable to LL2 or higher, such as higher excitons and states with two or more inter-LL excitations, whose FWM contribution is suppressed due to their small energetic overlap with the optical pulses and their enhanced dephasing. We note that a similar approximation in the many−body eigenstates is used in the literature since, in most cases, it describes the 2DEG excitation spectrum well.[26,27] It even becomes exact for very large magnetic fields, when the coulomb-to-cyclotron energy ratio $e^2/(\varepsilon l\omega_c^e)$ becomes smaller than 1 (ε is the dielectric constant). We note however that, in GaAs at 10T, $\omega_c \sim 18$ meV for electrons, while the characteristic Coulomb energy $e^2/\varepsilon l \sim 14$ meV. Therefore, for quantitative fits to experiments, one must include higher LLs.

Here we solve a polaronic problem where the LL0 (X_0) and LL1 (X_1) magnetoexcitons couple to a continuum of {1-LL0-e + 1-LL1-h + LL0→LL1MP} four-particle excitations (Y_q). In the case of X_1, the e-2DEG interaction scatters the LL1 electron to LL0 by emitting a LL0→LL1 2DEG excitation at small total energy cost. This resonant interaction process couples $|X_1\rangle$ to the continuum of orthonormal states[16]

$$|Y_q\rangle = \hat{Y}_q^\dagger|G\rangle = \hat{X}_{q01}^\dagger \hat{\rho}^e_{-q1\downarrow 0\uparrow}|G\rangle \tag{29}$$

where

$$\hat{\rho}^e_{q10\sigma} = \frac{1}{\sqrt{N}}\sum_k e^{iq_x k/\ell^2}\hat{e}^\dagger_{k+q_y/2\uparrow}\hat{e}_{k-q_y/2\sigma} \tag{30}$$

creates a LL0 → LL1 magnetoplasmon or magnetoroton[25,26] and

$$\hat{X}_{q01}^\dagger = \frac{1}{\sqrt{N}}\sum_k e^{iq_x/\ell^2}\hat{e}^\dagger_{k+q_y/2\downarrow}\hat{h}^\dagger_{-k+q_y/2\downarrow} \tag{31}$$

creates a {1-LL0-e + 1-LL1-h} interband excitation. In Y_q, the X_{01} and MP degrees of freedom have opposite momenta $\mathbf{q}$ and are strongly correlated. The analogy to the X−X correlation in undoped semiconductors[56] is clear. As we shall see, the dephasing of Y_q has an important effect on the optical response. X_0 also couples to the $|Y_q\rangle$ when its LL0 hole scatters to LL1. However, Y_q have higher energy than X_0 and thus the X_0−2DEG interactions are suppressed as compared to the X_1−2DEG interactions. This asymmetry between the two magnetoexcitons in the case of inter-LL MPs is important for understanding the experimentally observed dynamics.

Equations of Motion. We calculate the full dynamics within the subspace spanned by the 1−h+(N_e+1)−e states $|X_n\rangle$, n = 0,1, and $|Y_q\rangle$, eq 29. Different many−body effects are determined by the interaction matrix elements V_{nm}, W_{qn}, and $W_{qq'}$.

$$V_{nm} = \int \frac{d\mathbf{q}}{(2\pi)^2} v_q |\phi_{nm}(\mathbf{q})|^2 \tag{32}$$

determine the exciton binding energies (V_{nn}), static inter-LL coupling (V_{01}), and mean-field X−X interaction (V_{01}). The coupling between the X and Y states is determined by $W_{\mathbf{q}n} \propto v_{01}^{01}(\mathbf{q})$, where

$$v_{nn'}^{mm'}(q) = \frac{1}{2\pi l^2} v_q \phi^*_{mm'}(\mathbf{q})\phi_{nn'}(\mathbf{q}) \tag{33}$$

By setting $W_{\mathbf{q}n} = 0$ in our calculation, we decouple the Xs from the 2DEG and obtain an optical response similar to the undoped system.

$$W_{\mathbf{q}\mathbf{q}'} = 2v_{11}^{00}(\mathbf{q}'-\mathbf{q})\cos[(\mathbf{q}\times\mathbf{q}')_z l^2] - v_{11}^{11}(\mathbf{q}'-\mathbf{q}) - v_{00}^{00}(\mathbf{q}'-\mathbf{q}) \tag{34}$$

describes rescattering among the continuum of $Y_\mathbf{q}$ states, which corresponds to non−perturbative vertex corrections beyond the Born approximation.

The linear polarizations are obtained from eqs 7 and 8[16]

$$i\partial_t P_0^L = (\Omega_0 - i\Gamma_0)P_0^L - V_{01}P_1^L - d(t) - \frac{1}{\sqrt{N}}\sum_q v_{01}^{01}(\mathbf{q})\bar{P}_q^L \tag{35}$$

for the LL0 polarization and

$$i\partial_t P_1^L = (\Omega_1 - i\Gamma_1)P_1^L - V_{10}P_0^L - d(t) + \frac{1}{\sqrt{N}}\sum_\mathbf{q} v_{01}^{01}(\mathbf{q})\bar{P}_q^L \tag{36}$$

for the LL1 polarization, where the exciton dephasing rates, $\Gamma_0 = \Gamma_1 = 0.5$ meV, are chosen similar to the undoped system and the exciton energies are

$$\Omega_n = E_g + \left(n + \frac{1}{2}\right)(\omega_c^e + \omega_c^h) - V_{nn} \quad (37)$$

The equations of motion for the coherences between the ground state and the {1-LL0-e + 1-LL1-h + LL0→LL1MP} Y_q states are obtained from eq 8[16]

$$i\partial_t \overline{P}_q^L = (\overline{\Omega}_q - i\gamma)\overline{P}_q^L + \frac{v_{01}^{01}(q)}{\sqrt{N}}(P_1^L - P_0^L) + \frac{1}{N}\sum_{q' \neq q} W_{qq'}\overline{P}_{q'}^L \quad (38)$$

$\bar{\Omega}_q = \Omega_{q01} + \omega_{-q}$ is the Y_q dispersion, where $\Omega_{\mathbf{q}01}$ is the X_{01} excitation energy, shifted here by ∼1 meV as compared to its value in the ideal 2D system to obtain a better fit to the experimental linear absorption, and ω_q is the LL0→LL1 2DEG excitation energy, given at $\nu = 1$ by[24]

$$\omega_q - \omega_c^e = \frac{e^2}{\varepsilon\ell}\frac{q\ell}{2}e^{-q^2\ell^2/2} + \frac{e^2}{\varepsilon\ell}\frac{1}{2}\sqrt{\frac{\pi}{2}}\left\{1 - e^{-q^2\ell^2/4}\left[\left(1 + \frac{q^2\ell^2}{2}\right)I_0\left(\frac{q^2\ell^2}{4}\right) - \frac{q^2\ell^2}{2}I_1\left(\frac{q^2\ell^2}{4}\right)\right]\right\} \quad (39)$$

where I_n is a modified Bessel function of the first kind. The first term on the rhs of the above equation correponds to the RPA treatment of the 2DEG interactions. The second term results from the many-body corrections to the local field seen by an electron. These local field corrections result in a magnetoroton dispersion minimum absent within the RPA, whose detailed momentum dependence is determined by the ground state static structure factor.[26]

Next we present the equations of motion for the third-order nonlinear polarizations. Since the experimental studies of both doped and undoped quantum wells[38,39,66] did not produce any long-lasting FWM signal at negative time delays, which would signify long-lived X−X correlations,[1,56,59] we treat for simplicity the X−X interactions within the Hartree−Fock approximation. Within the chosen subspace of many-body states, the third-order polarization is described by the following closed system of equations of motion, derived in ref 16

$$i\partial_t P_0 - (\Omega_0 - i\Gamma_0)P_0 + V_{01}P_1 = d(t)n_0 + V_{01}P_1^L(n_0 - 2N_{01}^*) - V_{01}P_0^L(n_1 - 2N_{01}) - P_0^L\sum_q v_{01}^{01}(\mathbf{q})\left[\overline{n}_q + \frac{1}{\sqrt{N}}(M_{1\mathbf{q}}^* - M_{0\mathbf{q}})\right] - P_1^L\sum_q v_{01}^{01}(\mathbf{q})\left[\overline{n}_\mathbf{q} - \frac{1}{\sqrt{N}}(M_{1q} - M_{0q}^*)\right] - \frac{1}{\sqrt{N}}\sum_q v_{01}^{01}(\mathbf{q})P_0^L P_1^L\overline{P}_q^{L*} - \frac{1}{\sqrt{N}}\sum_q v_{01}^{01}(\mathbf{q})\overline{P}_q \quad (40)$$

$$i\partial_t P_1 - (\Omega_1 - i\Gamma_1)P_1 + V_{01}P_0 = d(t)n_1 - V_{01}P_1^L(n_0 - 2N_{01}^*) + V_{01}P_0^L(n_1 - 2N_{01}) + P_0^L\sum_q v_{01}^{01}(\mathbf{q})\left[\overline{n}_q + \frac{1}{\sqrt{N}}(M_{1q}^* - M_{0q})\right] + P_1^L\sum_q v_{01}^{01}(\mathbf{q})\left[\overline{n}_q - \frac{1}{\sqrt{N}}(M_{1q} - M_{0q}^*)\right] + \frac{1}{\sqrt{N}}\sum_q v_{01}^{01}(\mathbf{q})P_0^L P_1^L\overline{P}_q^{L*} + \frac{1}{\sqrt{N}}\sum_q v_{01}^{01}(\mathbf{q})\overline{P}_q \quad (41)$$

$\langle\hat{Y}_\mathbf{q}\rangle_{corr}$ is determined by the equation of motion

$$i\partial_t \overline{P}_q - (\overline{\Omega}_q - i\gamma)\overline{P}_q = \frac{v_{01}^{01}(\mathbf{q})}{\sqrt{N}}(P_1 - P_0) + \frac{1}{N}\sum_{q'} W_{qq'}\overline{P}_{q'} + d(t)(P_1^{L*} + P_0^{L*})\overline{P}_q^L + \frac{v_{01}^{01}(\mathbf{q})}{\sqrt{N}}[P_1^L(N_{11} - P_0^{L*}P_0^L - N_{00}) - P_0^L(N_{00} - P_1^{L*}P_1^L - N_{11})] + [v_{01}^{01}(\mathbf{q}) - V_{01}](P_1^L - P_0^L)(P_1^{L*}\overline{P}_q^L + M_{1q} - P_0^{L*}\overline{P}_q^L - M_{0q}) + \sum_{q'}\frac{v_{01}^{01}(\mathbf{q}')}{\sqrt{N}}\overline{P}_{q'}^L(M_{1q} - M_{0q}) + \frac{v_{01}^{01}(\mathbf{q})}{\sqrt{N}}(P_1^L - P_0^L)[2N\overline{n}_q - 3\sum_{q'}\overline{n}_{q'}] + (P_1^L - P_0^L)\sum_{q'}\frac{v_{01}^{01}(\mathbf{q}')}{\sqrt{N}}\overline{P}_{q'}^{L*}\overline{P}_q^L \quad (42)$$

where we neglected $Y_q \leftrightarrow Y_{q'}$ coherences by assuming that they dephase rapidly. We retain, however, the $X_n \leftrightarrow Y_q$ coherences M_{nq} and the $X_0 \leftrightarrow X_1$ coherence N_{01}, obtained from eqs 11 and 10 with dephasing rates of 0.5 meV. The nonlinearities in eqs 40, 41, and 42 depend on the total LLn carrier populations n_n and the Y−state populations $\bar{n}_q$

$$n_n = 2P_n^L P_n^{L*} + 2N_{nn} + \sum_q \overline{n}_q \quad (43)$$

where the first term is the coherent X_n population and the rest of the terms describe he incoherent LLn carrier population, with contributions N_{nn} and $\bar{n}_q$ from the X_n and Y_q states, respectively, where

$$\overline{n}_q = \overline{P}_q^{L*}\overline{P}_q^L + N_{qq} \quad (44)$$

N_{nn} and N_{qq} were obtained from eqs 10 and 12 with population relaxation rate $\Gamma_{qq} = \Gamma_{nn} = 0.001$ meV.

Numerical Results and Comparison to Experiment. In this section we present our numerical results, obtained for a magnetic field ∼9 T at $\nu = 1$, and compare them to the experiment. Figure 1 compares the linear absorption spectra calculated by using the full and RPA dispersions $\bar{\Omega}_\mathbf{q}$. It also compares the results obtained for a small, $\gamma = 0.35$ meV, and a large, $\gamma = 2\Gamma_1 = 2\Gamma_0 = 1$ meV, dephasing rate of the $Y_\mathbf{q}$ four-particle coherence, whose amplitude is $\bar{P}_\mathbf{q}$. Figure 1 demonstrates that the linear absorption line shape is sensitive to the Y_q dispersion. In particular, a second absorption peak, absent within the RPA, develops above the LL1 exciton resonance when the full Y_q dispersion is used. The latter displays a magnetoroton minimum, absent in the RPA dispersion, that is characteristic of incompressibility.[19,20,24−26] We note in Figure 1 that the double-peak LL1 resonance line shape depends sensitively on the dephasing of the {1-LL0-e + 1-LL1-h + LL0→LL1MP} four-particle correlation, characterized by γ. As γ increases, these correlations become short-lived and the two LL1 absorption peaks merge into one broad but asymmetric LL1 resonance. This result agrees with the experimental observation, shown in Figure 2. In contrast, the LL0 resonance is insensitive to the Y-state dynamics, consistent with the experiment (its precise line shape may however depend on intra-LL excitations[37,41]). γ can be large in the realistic system, due to, e.g., sample-dependent disorder- and phonon-induced scattering of the MP and X_{01} excitations, which have opposite momenta in $Y_\mathbf{q}$. On the other hand, the RPA line shape is less sensitive to γ, as seen in the inset of Figure 1, due to the absence of magnetorotons.

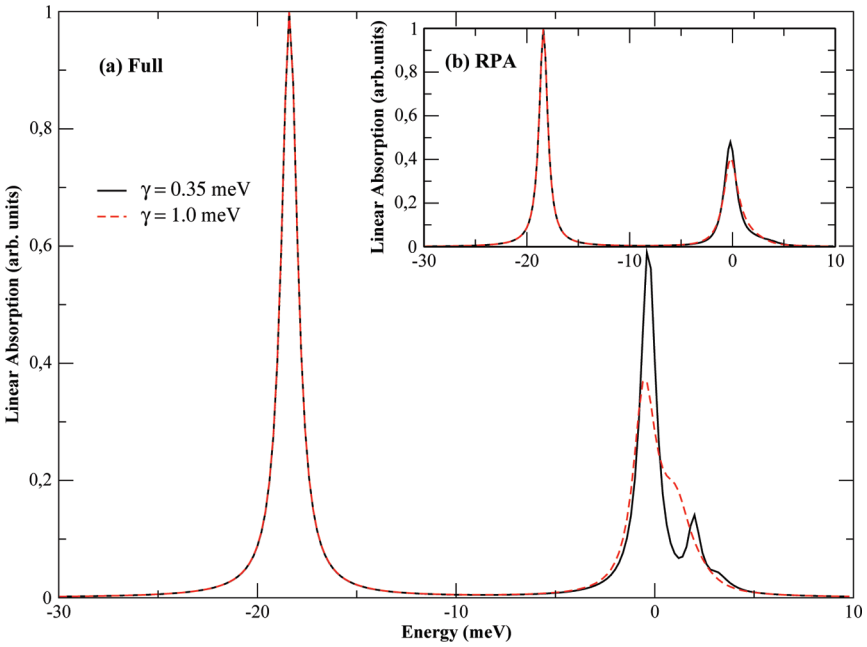

Figure 1. Linear absorption calculation using the full *Y*-state dispersion for two values of the *Y*-state dephasing rate γ. Inset: Same for the RPA *Y*-state dispersion.

Next we turn to the ultrafast nonlinear response to three time-delayed optical pulses

$$d(t) = \mu E_p(t)e^{i(\mathbf{k}_1 \cdot r - \omega_p t)} + \mu E_p(t + \Delta t_{12})e^{i(\mathbf{k}_2 \cdot r - \omega_p t)} + \mu E_p(t + \Delta t_{13})e^{i(\mathbf{k}_3 \cdot r - \omega_p t)} \quad (45)$$

where $E_p(t) = E_0 e^{-(t/t_p)^2}$ is the pulse amplitude and ω_p its central frequency. The optical fields propagate in the directions $\mathbf{k}_1$, $\mathbf{k}_2$, and $\mathbf{k}_3$, with a time delay Δt_{12} (Δt_{13}) between pulses $\mathbf{k}_1$ and $\mathbf{k}_2$ ($\mathbf{k}_3$). For negative time delays, pulse $\mathbf{k}_1$ arrives first. We calculate the FWM spectrum

$$S(\omega, \Delta t_{12}, \Delta t_{13}) = |P_0(\omega) + P_1(\omega)|^2 \quad (46)$$

in the background-free direction $\mathbf{k}_1 + \mathbf{k}_2 - \mathbf{k}_3$. By tuning ω_p close to LL1, the LL0/LL1 photoexcited carrier ratio n_0/n_1 is small. This suppresses the PSF contribution at the LL0 energy and highlights the interaction effects that distinguish the many-body system from a multi-level atomic-like system. Below we discuss the time-dependence obtained along the Δt_{12} axis ($\Delta t_{13} = 0$) and the Δt_{13} axis ($\Delta t_{12} = 0$), calculated in all cases at the two frequencies ω corresponding to the peaks of the LL0 and LL1 FWM resonances. For $\Delta t_{13} > 0$, $\Delta t_{12} = 0$, pulse $\mathbf{k}_3$ comes first and creates an interband polarization. The latter evolves and decays for a time interval Δt_{13}, when pulses $\mathbf{k}_1$ and $\mathbf{k}_2$ arrive and create the third-order FWM signal. Therefore, the $\Delta t_{13} > 0$ axis mainly accesses the polarization dephasing. Along the $\Delta t_{13} < 0$ axis, pulses $\mathbf{k}_1$ and $\mathbf{k}_2$ first create an X−X coherence, which evolves and dephases for a time-interval $|\Delta t_{13}|$ when pulse $\mathbf{k}_3$ arrives. Therefore, the $\Delta t_{13} < 0$ axis mainly accesses the dephasing of the X−X coherence. Along the negative Δt_{12} axis, pulses $\mathbf{k}_1$ and $\mathbf{k}_3$ arrive first ($\Delta t_{13} = 0$) and create a LL population, or a coherence between different X and Y states. These evolve and relax for a time interval $|\Delta t_{12}|$, at which time pulse $\mathbf{k}_2$ arrives. Therefore, the $\Delta t_{12} < 0$ axis probes population relaxation and intra-band coherence dephasing and oscillations. Finally, along the positive Δt_{12} axis, pulse $\mathbf{k}_2$ arrives first and creates an interband polarization, which evolves for a time interval Δt_{12} when pulses $\mathbf{k}_1$ and $\mathbf{k}_3$ arrive. Thus the $\Delta t_{12} > 0$ axis mainly probes polarization dephasing. The FWM dependence on the two time delays gives complementary information on the coherent and relaxation dynamics of the QHS.

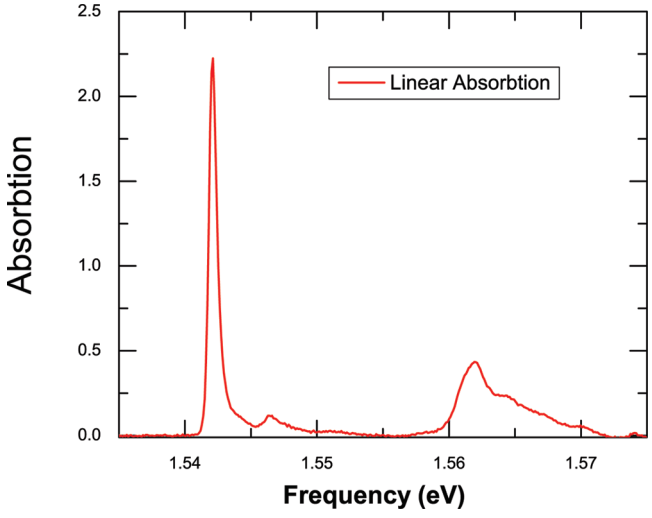

Figure 2. Experimental linear absorption.

Figure 3 shows the three-pulse FWM signal, calculated at the LL0 and LL1 FWM peak energies, for linear absorption as in Figure 1. We compare the results obtained for small and large dephasing rate γ of the {1-LL0-e + 1-LL1-h + LL0→LL1MP} correlations as in Figure 1. Despite tuning the frequency ω_p close to LL1, for small γ the LL0 and LL1 FWM peaks have comparable height. By increasing γ, the LL1/LL0 FWM peak ratio decreases sharply, as the two LL1 linear absorption peaks begin to merge into a single broad resonance. On the other hand, the LL0 peak remains relatively insensitive to γ and $\bar{P}_q$. Regarding the time-dependence, along the Δt_{12} axis the LL0 FWM signal

dx.doi.org/10.1021/jp1118794 |*J. Phys. Chem. B* 2011, 115, 5634–5647

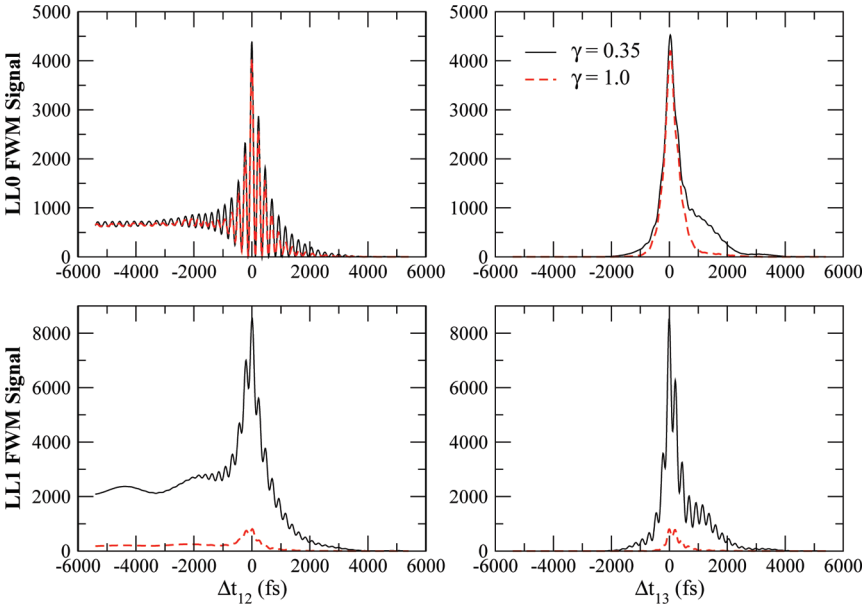

Figure 3. Calculated three-pulse FWM signal and its dependence on the {1-LL0-e + 1-LL1-h + LL0→LL1MP} correlation dephasing.

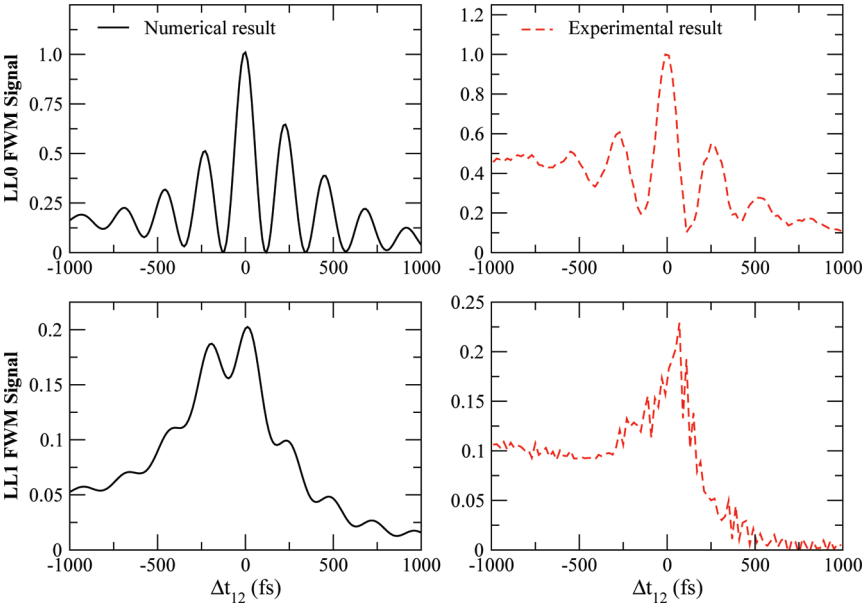

Figure 4. Three-pulse FWM: comparison between theory and experiment along the Δt_{12} axis for γ = 1 meV.

displays strong temporal coherent oscillations, with a frequency determined by the LL0−LL1 energy splitting. Importantly, the decay of these oscillations is enhanced by increasing γ, which indicates that it is determined by dephasing due to X−2DEG interactions. Along the $\Delta t_{13} > 0$ axis, for small γ the FWM temporal profile displays a small oscillation. With increasing γ however, the LL0 temporal profile becomes symmetric around $\Delta t_{13} = 0$, as the two linear absorption LL1 peaks merge into a single broad resonance, while the LL1 temporal profile remains asymmetric. The dependence of the above features on the {1-LL0-e + 1-LL1-h + LL0→LL1MP} dephasing rate γ indicates that they arise from non-Markovian memory effects due to the four-particle correlations and their dynamics. Furthermore, along the $\Delta t_{12} < 0$ axis, the FWM signal reflects the relaxation of the incoherent carrier populations and decreases drastically if we neglect the long−lived incoherent Y-state populations N_{qq}.[16] The FWM spectral and temporal profile can be controlled by tuning ω_p toward the LL0 frequency, which suppresses the LL1 FWM peak.

We now compare our predictions to the FWM experiments discussed in refs 38, 39, and 66. We take γ = 1 meV, which gives good agreement between the theoretical and experimental linear absorption if we ignore the extra peaks due to the valence bandstructure (compare Figures 1 and 2). Figure 4 compares the FWM time evolution along the Δt_{12} axis. Our theory captures the main experimental features: strong LL0 temporal oscillations due to LL0−LL1 coherence, $\Delta t_{12} < 0$ signal reflecting incoherent population relaxation, and unusually large LL0/LL1 peak ratio

dx.doi.org/10.1021/jp1118794 |J. Phys. Chem. B 2011, 115, 5634–5647

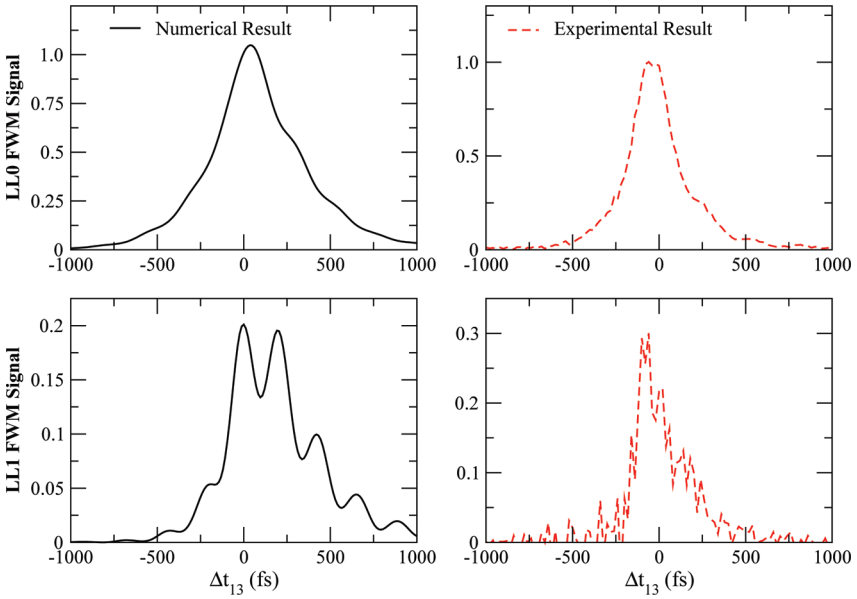

Figure 5. Three-pulse FWM: comparison between theory and experiment along the Δt_{12} axis for $\gamma = 1$ meV.

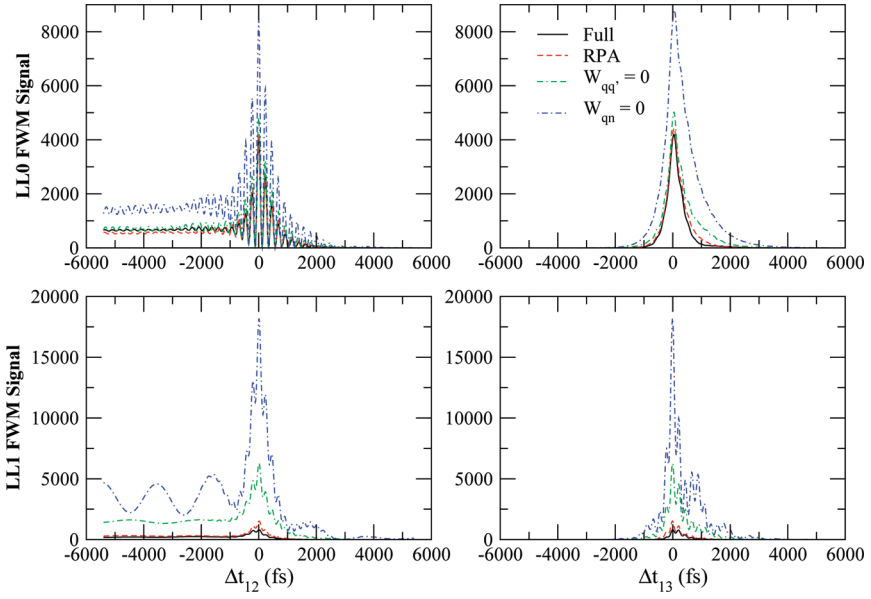

Figure 6. Interaction effects on the three-pulse FWM signal for $\gamma = 1$ meV.

despite predominantly exciting LL1 transitions. Figure 5 compares the calculated and experimental temporal evolution along the Δt_{13} axis. We capture the symmetric LL0 temporal profile seen in the experiment, absent in the undoped system,[66] while the time-dependence of the LL1 FWM is asymmetric around $\Delta t_{13} = 0$. Our theory predicts the experimentally-observed FWM features of the 2DEG which are absent in an atomic-like or an undoped semiconductor system.

Next we discuss the origin of the above effects. Figure 6 compares our full calculation to the result obtained by setting $W_{qn} = 0$, in which case the X states decouple from the 2DEG. While the full calculation gives a large LL0/LL1 FWM ratio (LL0/LL1∼5), this ratio is strongly suppressed if we set $W_{qn} = 0$ (LL0/LL1∼1/2). This rather drastic effect of the X−2DEG coupling is consistent with the observed differences between the 2DEG and undoped samples.[38,39,66] Furthermore, for $W_{qn} = 0$, the LL0 FWM temporal profile along the Δt_{13} axis becomes asymmetric, as observed in the undoped system.[66] Along the Δt_{12} axis, coherent oscillations are also present for $W_{qn} = 0$, attributed to the X−X interactions.[66] However, while in the undoped system the oscillation decay is determined by the exciton dephasing rates Γ_n, in the 2DEG it mainly comes from X−2DEG interactions and the dynamics of the Y states. While the profound role of the X−2DEG coupling in interpreting the experiment is clear from the results of Figure 6, we note that, with increasing γ, the differences[16] between the RPA and the full Y_q dispersion FWM calculations decrease. This result suggests that the incompressibility of the 2DEG does not strongly affect the FWM in the samples studied here due to strong dephasing of the {1-LL0-e + 1-LL1-h + LL0→LL1MP} correlation.

dx.doi.org/10.1021/jp1118794 |J. Phys. Chem. B 2011, 115, 5634–5647

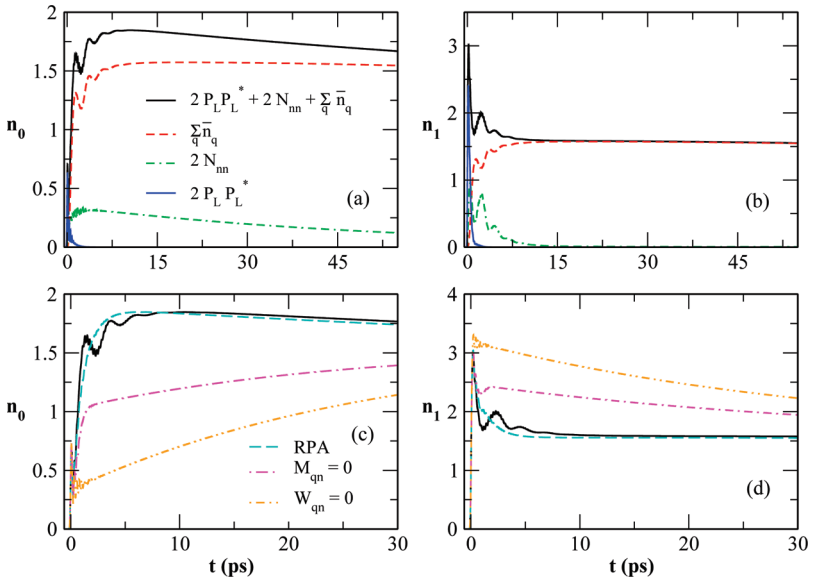

Figure 7. LL0 and LL1 total carrier population relaxation for photoexcitation close to LL1 by a single pulse and $\gamma = 1$ meV. Upper panel: time evolution of the different coherent and incoherent contributions. Lower panel: comparison between populations obtained with the full calculation, RPA dispersion, and by neglecting the linear or nonlinear X−Y couplings.

To interpret the unusual temporal profile along the Δt_{13} axis and its dependence on γ, let us consider the PSF and X−X interaction contributions to eqs 40 and 41. The PSF contribution, $d(t)n_n$ at LLn, always gives an asymmetric Δt_{13} temporal profile, with $\Delta t_{13} < 0$ contribution that follows the optical pulse.[2,4] At LL0, the resonant X−X interaction contribution in eq 40 has the form $P_0^L n_1$ and $P_1^L N_{01}{}^*$, which couples the two LLs via light-induced nonlinear coherence. The $\Delta t_{13} > 0$ decay of the LL0 FWM signal then reflects the dephasing of X_1, while its $\Delta t_{13} < 0$ decay reflects the dephasing of the $X_1 + X_0$ coherence. X_1 couples strongly to the $Y_{\mathbf{q}}$ states in the QHS and thus dephases more strongly than X_0. If γ is sufficiently large, so that the LL1 resonance is broad, the Δt_{13} temporal profile is dominated by the dephasing of P_1^L. If on the other hand γ is small, P_1^L is long lived and the temporal profile becomes asymmetric, with memory effects due to the multi-peak structure in Figure 1. When $W_{\mathbf{q}n} = 0$, both X_0 and X_1 have similar dephasing rates and thus the Δt_{13} temporal profile is again asymmetric. In contrast, at the LL1 energy, the X−X interaction resonant contribution has the form $P_1^L n_0$ and $P_0^L N_{01}$. Therefore, while the $\Delta t_{13} < 0$ FWM decay again reflects the $X_0 + X_1$ dephasing, the $\Delta t_{13} > 0$ FWM signal is determined by the dephasing of X_0 and thus decays more slowly than the LL0 FWM, since X_0 couples weakly to inter-LL MPs. We conclude that the observation of a symmetric LL0 Δt_{13} profile reflects the asymmetry in the dephasing of the LL0 and LL1 excitons due to coupling with inter-LL MPs. Even though the X−X interaction + PSF nonlinear contribution gives a large part of the 2DEG FWM,[16] it still gives a LL1/LL0 ratio much larger than the full calculation, while its dynamics changes drastically when $W_{\mathbf{q}n} \neq 0$.

The question now arises whether a perturbative Born approximation treatment of the X−2DEG interactions and the corresponding exciton self−energy is enough to describe the above effects. Figure 6 compares our full calculation to the Born approximation result, obtained by setting $W_{\mathbf{q}\mathbf{q}'} = 0$ in eq 42. This approximation neglects the scattering between the X_{01} and MP excitations that make $Y_{\mathbf{q}}$. This X_{01}−MP dynamics is similar to that due to X−X scattering in the undoped system, which governs the dynamics of the four-particle 2−h+2−e correlation and the $\Delta t_{13} < 0$ FWM signal.[56,59] Figure 6 shows that the perturbative treatment of the X−2DEG scattering significantly overestimates the strength of the LL1 peak, by a factor of more than ∼5 as compared to the full calculation. Importantly, it gives a more asymmetric Δt_{13} temporal profile and also changes the decay of the $\Delta t_{12} < 0$ LL0 temporal oscillations. We conclude that the vertex (rescattering) corrections affect the FWM profile in a significant way. In particular, the non−exponential time−dependence of the {1-LL0-e + 1-LL1-h + LL0→LL1MP} correlation manifests itself in the symmetric temporal profile of the Δt_{13} signal, which is not adequately described by the Born approximation or by the average polarization model used to inerpret the 2DEG FWM experiments.[15,39,43−46]

We now turn to the population relaxation. Figure 7, panels a and b, shows the time evolution of the LL0 (n_0) and LL1 (n_1) total carrier populations, photoexcited at $t = 0$ by a single optical pulse, and their different contributions,.[43] The coherent contribution to n_n, $2P_n^L P_n^{L*}$, decays rapidly, as determined by the polarization dephasing. When ω_p is tuned close to the LL1 energy, the coherent n_1 exceeds n_0, by a factor ∼4 in Figure 7. Nevertheless, it is clear from our results that the LL0/LL1 FWM ratio does not simply reflect the ratio n_0/n_1, in contrast to the predictions of a multi-level atomic-like model. Following the coherent regime, the X−2DEG interaction drastically changes the carrier relaxation and enhances n_0/n_1 as compared to the undoped system. The LL0 population increases sharply during intermediate time scales of a few picoseconds, while simultaneously the LL1 population drops and the Y-state populations build up. This incoherent dynamics comes from the $X_1 \rightarrow Y_{\mathbf{q}}$ scattering processes. It is described by eqs 10, 11, and 12 and should be contrasted to the coherent dynamics due to the same interaction process, discussed above. The rise time of the LL0 FWM signal for $\Delta t_{12} < 0$ mainly reflects the slow build-up of the Y-state populations $\Sigma_{\mathbf{q}} \bar{n}_{\mathbf{q}}(t)$ as X_1 depopulates. Figure 7, panels a and b, also shows the time-dependence of the incoherent exciton

dx.doi.org/10.1021/jp1118794 |J. Phys. Chem. B 2011, 115, 5634–5647

populations $N_{nn}(t)$. N_{00} relaxes slowly, as determined by the population relaxation time, since the X_0 + 2DEG scattering is suppressed for inter-LL MPs. In contrast, the relaxation of N_{11} is fast and occurs on a time scale of a few picoseconds, which coincides with the build-up of $\bar{n}_{\mathbf{q}}$. After sufficiently long times, when the above scattering is complete, n_n are determined by the total population of the continuum of {1MP + 1-LL0-e + 1-LL1-h} states and by the long−lived LL0 population N_{00}. Finally, Figure 7, panels c and d, compares the n_n obtained by using the full or the RPA $Y_{\mathbf{q}}$ dispersions and show rather small differences between them. In contrast, by neglecting the linear or nonlinear X−Y couplings, i.e., by setting $W_{\mathbf{q}n} = 0$ or $M_{\mathbf{q}n} = 0$, we obtain drastically different population relaxation and time-dependence of n_0/n_1.

CONCLUSIONS

In conclusion, we developed a density matrix quantum kinetic description of dephasing/decoherence and relaxation processes in photoexcited systems with strongly correlated ground state electrons. Similar to the description of the strongly correlated QH ground state and its excitations (composite fermions etc),[27,30,55] in the absence of a small interaction parameter, we obtain the exact dynamics of "Hubbard operator" density matrices within a subspace of almost degenerate many-body states strongly coupled by the interactions, after introducing an appropriate density matrix decomposition that separates different correlation effects. Our main motivation for developing this theory is to address the timely, both from nonequilibrium many-body physics and from applications points of view, problem of nonlinear dynamics induced by the strong coupling of different degrees of freedom triggered by coherent photoexcitation. We compared the predictions of our theory to three-pulse FWM experiments, performed on a 2DEG subjected to a magnetic field. This comparison corroborates our earlier claims that the dynamical coupling of the two lowest Landau level states by inter-LL magnetoplasmon (MP) and magnetoroton (MR) 2DEG excitations is an important and robust nonlinear process in the QHS, with possible implications for coherent control and quantum computation schemes involving many-body qubits. Importantly, we showed that the spectral and temporal behavior of the FWM signal depends sensitively on the dephasing and dynamics of {1-LL0-e + 1-LL1-h + LL0→LL1MR} four-particle correlations, which couple to the exciton degrees of freedom. For long-lived correlations, the incompressibility of the 2DEG, which leads to magnetorotons and a double-peak LL1 resonance, manifests itself in the FWM profile. For short-lived correlations, the dephasing of the LL1 coherence is strong, leading to an unusually symmetric temporal profile, determined by the dynamics of the above four-particle correlations, and a depressed LL1 FWM peak. These correlations also affect the decay of the inter-LL coherence that gives FWM temporal oscillations, which in the undoped system is determined by the exciton dephasing rates. A question down the road is how two-dimensional correlation spectroscopy,[67] which accesses a much larger phase space than the conventional one-dimensional spectroscopic techniques, can be used to resolve the dynamics of such fundamental many-body processes. Future experimental and theoretical studies also promise to elucidate the dynamics of strongly coupled spin, charge, and lattice degrees of freedom that is triggered by coherent photoexcitation of selected modes. In addition to accessing "hidden states" and photo-induced phase transitions in strongly correlated materials, such studies of the QHS can address, for example, the formation and nonlinear response dynamics of trions, composite fermions, and fractional quasi-excitons.[30,51,55]

AUTHOR INFORMATION

Corresponding Author
*E-mail: ilias@physics.uoc.gr.

ACKNOWLEDGMENT

This work was supported by the EU ITN program ICARUS.

REFERENCES

(1) Chemla, D. S.; Shah, J., *Nature* **2001**, *411*, 549. Chemla, D. S. In *Non-linear Optics in Semiconductors*; Willardson, R. K., Beers, A. C., Eds.; Academic Press: New York, 1999.
(2) Schäfer, W.; Wegener, M. *Semiconductor Optics and Transport Phenomena*; Springer: Berlin, 2002.
(3) Mukamel, S. *Principles of Nonlinear Optical Spectroscopy*; Oxford University Press: New York, 1995.
(4) Shah, J., *Ultrafast Spectroscopy of Semiconductors and Semiconductor Nanostructures, Vol. 115 of Springer Series in Solid--State Sciences*, Springer-Verlag, Berlin Heidelberg New York, 2nd ed. (1999).
(5) Haug, H.; Koch, S. W., *Quantum Theory of the Optical and Electronic Properties of Semiconductors*, World Scientific (1993).
(6) Abramavicius, D.; Palmieri, B.; Voronine, D. V.; Sanda, F.; Mukamel, S. *Chem. Rev* **2009**, *109*, 2350. Mukamel, S.; Abramavicius, D. *Chem. Rev.* **2004**, *104*, 2073.
(7) Turner, D. B.; Nelson, K. A. *Nature* **2010**, *466*, 1089.
(8) Rossi, F.; Kuhn, T. *Rev. Mod. Phys.* **2002**, *74*, 895.
(9) Axt, V. M.; Stahl, A. Z. *Phys. B Condens. Matter* **1994**, *93*, 195. Victor, K.; Axt, V. M.; Stahl, A. *Phys. Rev. B* **1995**, *51*, 14164.
(10) Axt, V. M.; Victor, K.; Stahl, A. *Phys. Rev. B* **1996**, *53* (11), 7244.
(11) Axt, V. M.; Mukamel, S. *Rev. Mod. Phys.* **1998**, *70*, 145.
(12) Perakis, I. E.; Shahbazyan, T. V. *Surf. Sci. Rep.* **2000**, *40*, 1. Perakis, I. E.; Shahbazyan, T. V. *Int. J. Mod. Phys. B* **1999**, *13*, 869. Perakis, I. E. *Chem. Phys.* **1996**, *210*, 259.
(13) Perakis, I. E.; Chemla, D. S. *Phys. Rev. Lett.* **1994**, *72*, 3202. Shahbazyan, T. V.; Primozich, N.; Perakis, I. E.; Chemla, D. S. *Phys. Rev. Lett.* **2000**, *84*, 2006. Primozich, N.; Shahbazyan, T. V.; Perakis, I. E.; Chemla, D. S. *Phys. Rev. B* **2000**, *61*, 2041.
(14) Brener, I.; Knox, W. H.; Schäefer, W. *Phys. Rev. B* **1995**, *51*, 2005. Perakis, I. E.; Brener, I.; Knox, W. H.; Chemla, D. S. *J. Opt. Soc. Am. B* **1996**, *13*, 1313.
(15) Karathanos, A. T.; Perakis, I. E.; Fromer, N. A.; Chemla, D. S. *Phys. Rev. B* **2003**, *67*, 035316.
(16) Karadimitriou, M. E.; Kavousanaki, E. G.; Perakis, I. E.; Dani, K. M. *Phys. Rev. B* **2010**, *82*, 165313.
(17) Nasu, K. *Photoinduced Phase Transitions*; World Scientific: Singapore, 2004.
(18) See e.g.: Polli, D.; et al. *Nat. Mater.* **2007**, *6*, 643. Rini, M.; et al. *Nature* **2007**, *449*, 72. Fiebig, M.; et al. *Science* **1998**, *280*, 1925.
(19) Chakraborty, T.; Pietilainen, P., *The Quantum Hall Effects, Fractional and Integral*, 2nd ed.; Springer: New York, 1995.
(20) Yoshioka, D. *The Quantum Hall Effect, Vol. 133 of Springer Series in Solid−State Sciences*; Springer−Verlag: Berlin, 2002.
(21) Pinczuk, A. *Perspectives in Quantum Hall Effects:Novel Quantum Liquids in Low-Dimensional Semiconductor Structures*; Wiley: New York, 1996; Chapter 8.
(22) Laughlin, R. B. *Phys. Rev. Lett.* **1983**, *50*, 1395.
(23) Pinczuk, A.; Valladares, J. P.; Heiman, D.; Gossard, A. C.; English, J. H.; Tu, C. W.; Pfeiffer, L; West, K *Phys. Rev. Lett.* **1988**, *61*, 2701. Pinczuk, A.; Dennis, B. S.; Pfeiffer, L. N.; West, K. *Phys. Rev.*

Lett. **1993**, *70*, 3983. Eriksson, M. A.; Pinczuk, A.; Dennis, B. S.; Simon, S. H.; Pfeiffer, L. N.; West, K. W. *Phys. Rev. Lett.* **1999**, *82*, 2163.
(24) Kallin, C.; Halperin, B. I. *Phys. Rev. B* **1984**, *30* (10), 5655.
(25) Girvin, S. M.; MacDonald, A. H.; Platzman, P. M. *Phys. Rev. Lett.* **1985**, *54*, 581.
(26) MacDonald, A. H.; Oji, H. C. A.; Girvin, S. M. *Phys. Rev. Lett.* **1985**, *55*, 2208. Oji, H. C. A.; MacDonald, A. H. *Phys. Rev. B* **1986**, *33* (6), 3810. MacDonald, A. H. *J. Phys. C Solid State Phys.* **1985**, *18* (5), 1003.
(27) Kamilla, R. K.; Wu, X. G.; Jain, J. K. *Phys. Rev. B* **1996**, *54*, 4873.
(28) Jain, J. K. *Phys. Rev. Lett.* **1989**, *63*, 199; *Phys. Today* **2000**, *53* (4), 39.
(29) Stormer, H. L.; Tsui, D. C.; Gossard, A. C. *Rev. Mod. Phys.* **1999**, *71*, S298.
(30) Wójs, A.; Gladysiewicz,and, A.; Quinn, J. J. *Phys. Rev. B* **2006**, *73*, 235338. Byszewski, M.; Chwalisz, B.; Maude, D. K.; Sadowski, M. L.; Potemski, M.; Saku, T.; Hirayama, Y.; Studenikin, S.; Austing, D. G.; Sachrajda, A. S.; Hawrylak, P. *Nat. Phys.* **2006**, *2*, 239.
(31) Sinova, J.; MacDonald, A. H.; Girvin, S. M. *Phys. Rev. B* **2000**, *62*, 13579.
(32) Rezayi, E. H. *Phys. Rev. B* **1987**, *36*, 5454; **1991**, *43*, 5944.
(33) Sondhi, S. L.; Karlhede, A.; Kivelson, S A.; Rezayi, E. H. *Phys. Rev. B* **1993**, *47*, 16419.
(34) MacDonald, A. H.; Fertig, H. A.; Brey, L. *Phys. Rev. Lett.* **1996**, *76*, 2153. Fertig, H. A.; Brey, L.; Côté, R.; MacDonald, A. H. *Phys. Rev. B* **1994**, *50*, 11018. Fertig, H. A.; Brey, L.; Côté, R.; MacDonald, A. H.; Karlhede, A.; Sondhi, S. L. *Phys. Rev. B* **1997**, *55*, 10671.
(35) Barrett, S. E.; Dabbagh, G.; Pfeiffer, L. N.; West, K. W.; Tycko, R. *Phys. Rev. Lett.* **1995**, *74*, 5112. Tycko, R.; Barrett, S. E.; Dabbagh, G.; Pfeiffer, L. N.; West, K. W. *Science* **1995**, *268*, 1460.
(36) Das Sarma, S.; Freedman, M.; Nayak, C. *Phys. Rev. Lett.* **2005**, *94*, 166802.
(37) Fromer, N. A.; Schüller, C.; Chemla, D. S.; Shahbazyan, T. V.; Perakis, I. E.; Maranowski, K.; Gossard, A. C. *Phys. Rev. Lett.* **1999**, *83*, 4646.
(38) Fromer, N. A.; Lai, C. E.; Chemla, D. S.; Perakis, I. E.; Driscoll, D.; Gossard, A. C. *Phys. Rev. Lett.* **2002**, *89*, 067401.
(39) Dani, K. M.; Tignon, J.; Breit, M.; Chemla, D. S.; Kavousanaki, E. G.; Perakis, I. E. *Phys. Rev. Lett.* **2006**, *97*, 057401.
(40) Fromer, N. A.; Schüller, C.; Lai, C. W.; Chemla, D. S.; Perakis, I. E.; Driscoll, D.; Gossard, A. C. *Phys. Rev. B* **2002**, *66*, 205314.
(41) Schüller, C., Perakis, I. E., Fromer, N. A., Chemla, D. S. In *Nonequilibrium Physics at Short Time Scales: Formation of Correlations*; Morawetz, K., Ed.; Springer Verlag: Berlin, 2004; pp 209.
(42) Dani, K. M.; Tignon, J.; Breit, M.; Chemla, D. S.; Kavousanaki, E. G.; Perakis, I. E. *Physica E* **2006**, *34*, 206.
(43) Perakis, I. E.; Chemla, D. S. *Phys. Status Solidi (b)* **2002**, *234*, 242. Perakis, I. E. *Phys. Status Solidi (b)* **2003**, *238*, 502. Perakis, I. E.; Chemla, D. S. *Solid State Commun.* **2003**, *127*, 147.
(44) Perakis, I. E.; Kavousanaki, E. G. *Chem. Phys.* **2005**, *318*, 118.
(45) Dani, K. M.; Kavousanaki, E. G.; Tignon, J.; Chemla, D. S.; Perakis, I. E. *Solid State Commun.* **2006**, *140*, 72.
(46) Kavousanaki, E. G.; Dani, K. M.; Tignon, J.; Chemla, D. S.; Perakis, I. E. *Phys. Status Solidi (b)* **2006**, *243*, 2397.
(47) Hubbard, J. *Proc. R. Soc. London A* **1965**, *285*, 542.
(48) Ruckenstein, A. E.; Schmitt-Rink, S. *Int. J. Mod. Phys. B* **1989**, *3*, 1809; Igarashi, J. *J. Phys. Soc. Jpn.* **1983**, *52*, 2827; **1985**, *54*, 260. Igarashi, J.; Takahashi, M.; Nagao, T. *J. Phys. Soc. Jpn.* **1999**, *68*, 3682.
(49) Kapetanakis, M. D.; Perakis, I. E. *Phys. Rev. B* **2008**, *78*, 155110. Kapetanakis, M. D.; Perakis, I. E. *Phys. Rev. B* **2007**, *75*, 140401(R). Kapetanakis, M. D.; Manousaki, A.; Perakis, I. E. *Phys. Rev. B* **2006**, *73*, 174424. Kapetanakis, M. D.; Perakis, I. E. *Phys. Rev. Lett.* **2008**, *101*, 097201.
(50) Östreich, T.; Schönhammer, K.; Sham, L. J. *Phys. Rev. Lett.* **1995**, *74*, 4698. Östreich, T.; Schönhammer, K.; Sham, L. J. *Phys. Rev. B* **1998**, *58*, 12920.
(51) Broocks, K.-B.; Su, B.; Schröter, P.; Heyn, Ch.; Heitmann, D.; Wegscheider, W.; Apalkov, V. M.; Chakraborty, T.; Perakis, I. E.; Schüller, C. *Phys. Status Solidi (b)* **2008**, *245*, 321.
(52) Groshaus, J. G.; Umansky, V.; Shrtrikman, H.; Levinson, Y.; Bar−Joseph, I. *Phys. Rev. Lett.* **2004**, *93*, 096802. Yusa, G.; Shtrikman, H.; Bar−Joseph, I. *Phys. Rev. Lett.* **2001**, *87*, 216402.
(53) Yakovlev, D. R.; Kochereshko, V. P.; Suris, R. A.; Schenk, H.; Ossau, W.; Waag, A.; Landwehr, G.; Christianen, P. C. M.; Maan, J. C. *Phys. Rev. Lett.* **1997**, *79*, 3974.
(54) Schüller, C.; Broocks, K.−B.; Heyn, Ch.; Heitmann, D. *Phys. Rev. B* **2002**, *65*, 081301(R).
(55) Wójs, A.; Quinn, J. J.; Hawrylak, P. *Phys. Rev. B* **2000**, *62*, 4630. Gladysiewicz, A.; Bryja, L.; Wójs., A.; Potemski, M. *Phys. Rev. B* **2006**, *74*, 115332.
(56) Kner, P.; Bar-Ad, S.; Marquezini, M. V.; Chemla, D. S.; Schäfer, W. *Phys. Rev. Lett.* **1997**, *78*, 1319. Kner, R. L. P.; Schäfer, W.; Chemla, D. S. *Phys. Rev. Lett.* **1998**, *81*, 5386.
(57) Kotliar, G.; Savrasov, S. Y.; Haule, K.; Oudovenko, V. S.; Parcollet, O.; Marianetti, C. A. *Rev. Mod. Phys.* **2006**, *78*, 865.
(58) Kapetanakis, M. D.; Perakis, I. E.; Wickey, K. J.; Piermarocchi, C.; Wang, J. *Phys. Rev. Lett.* **2009**, *103*, 047404.
(59) Shahbazyan, T. V.; Primozich, N.; Perakis, I. E. *Phys. Rev. B* **2000**, *62*, 15925.
(60) Park, T. J.; Light, J. C. *J. Chem. Phys.* **1986**, *85*, 5870.
(61) Dzyubenko, A. B; Yu. Sivachenko, A. *Phys. Rev. Lett.* **2000**, *84*, 4429. Dzyubenko, A. B. *Phys. Rev. B* **2004**, *69*, 115332.
(62) Lerner, I. V.; Lozovik, Yu. E. *Zh. Eksp. Teor. Fiz.* **1981**, *80*, 1488; *Sov. Phys. JETP* **1981**, *53*, 763. MacDonald, A. H.; Rezayi, E. H. *Phys. Rev. B* **1990**, *42*, R3224.
(63) Apalkov, V. M.; Rashba, E. I. *Phys. Rev. B* **1992**, *46* (3), 1628. Apalkov, V. M.; Rashba, E. I. *Phys. Rev. B* **1993**, *48*, 18312.
(64) Cooper, N. R.; Chklovskii, D. B. *Phys. Rev. B* **1997**, *55*, 2436.
(65) Aifer, E. H.; Goldberg, B. B.; Broido, D. A. *Phys. Rev. Lett.* **1996**, *76*, 680.
(66) Dani, K. M.; Cotoros, I. A.; Wang, J.; Tignon, J.; Chemla, D. S.; Kavousanaki, E. G.; Perakis, I. E. *Phys Rev B* **2008**, *78*, R041301.
(67) Yang, L.; Mukamel, S. *Phys. Rev. Lett.* **2008**, *100*, 057402. Yang, L.; Zhang, T.; Bristow, A. D.; Cundiff, S. T.; Mukamel, S. *J. Chem. Phys.* **2008**, *129*, 234711. Yang, L.; Schweigert, I. V.; Cundiff, S. T.; Mukamel, S. *Phys. Rev. B* **2007**, *75*, 125302.